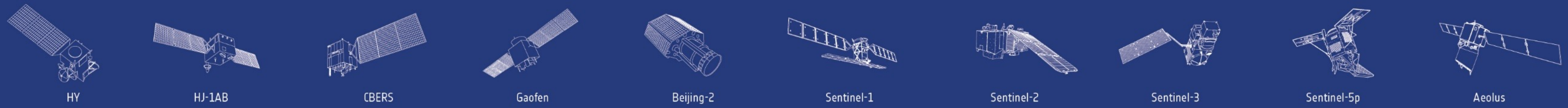

2023 DRAGON 5 SYMPOSIUM

3rd YEAR RESULTS REPORTING

11-15 SEPTEMBER 2023

[PROJECT ID. 57457]

[SINO-EU OPTICAL DATA TO PREDICT AGRONOMICAL VARIABLES AND TO MONITOR AND FORECAST CROP PESTS AND DISEASES]

13 SEPTEMBER, 2023, ID. S.6.3

ID. 57457

PROJECT TITLE: APPLICATION OF SINO-EU OPTICAL DATA INTO AGRONOMIC MODELS TO PREDICT CROP PERFORMANCE AND TO MONITOR AND FORECAST CROP PESTS AND DISEASES

PRINCIPAL INVESTIGATORS: [STEFANO PIGNATTI MORANO, WENJIANG HUANG**]**

CO-AUTHORS: [GUIJUN YANG, G. LANEVE, R. CASA**]**

PRESENTED BY: [STEFANO PIGNATTI MORANO**]**

Context

In recent years, newly launched satellites have achieved multi-satellite networking, meter-level spatial resolution, and a global revisit cycle of 2-5 days

Better than meters spatial resolution, 2-5 days short revisit

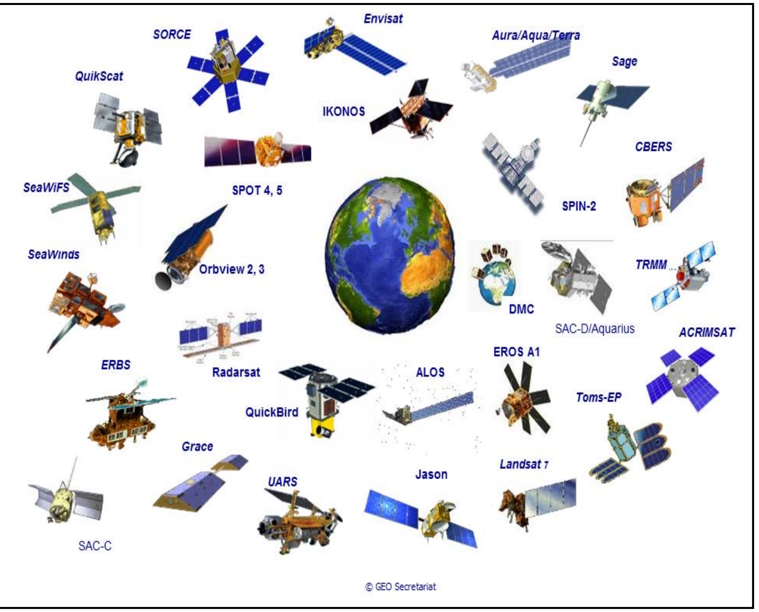

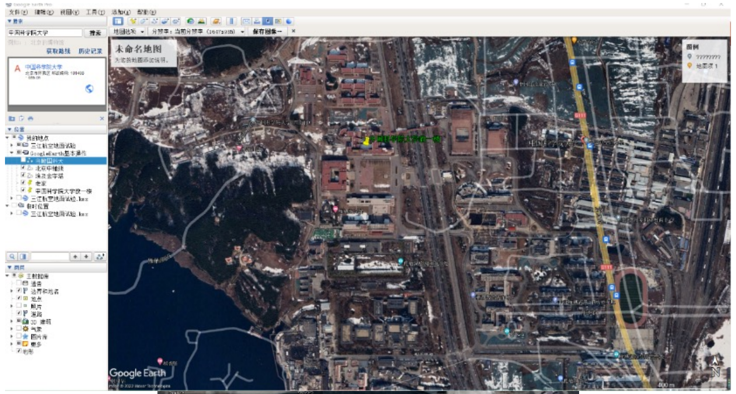

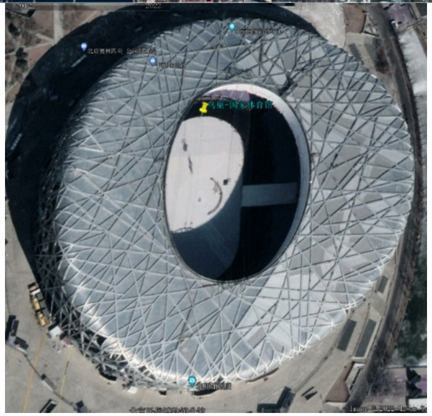

CEOS, ESA , NASA, NRSCC pay more attention on remote sensing applications

The Committee on Earth Observation Satellites

European Space Agency

Context

Remote sensing due to its high spatial resolution (meters), high temporal (2-5 Days revisit), hyperspectral (hundreds bands) advantages in vegetation is suitable for monitoring, forecasting, and assessing crop growth, diseases, pests, and yield

Plant distribution & phenology

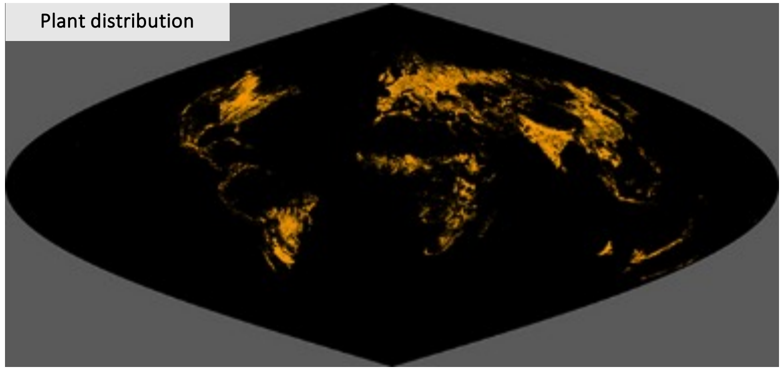

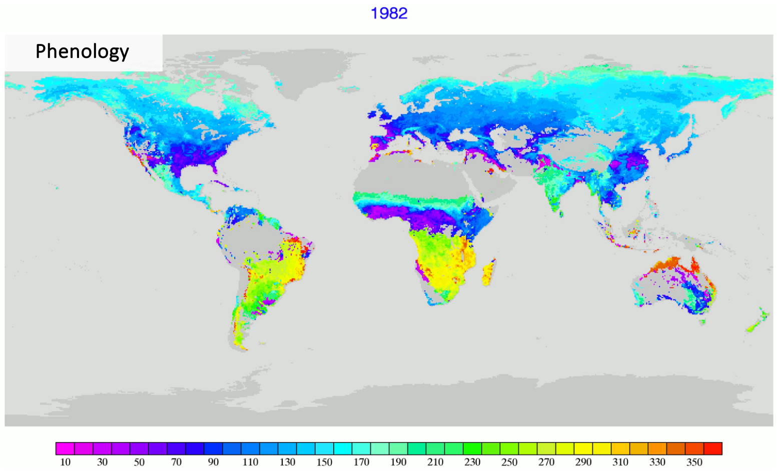

Environmental factors

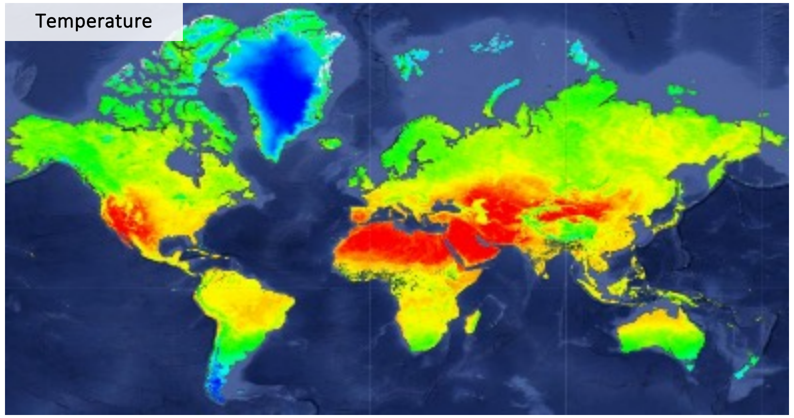

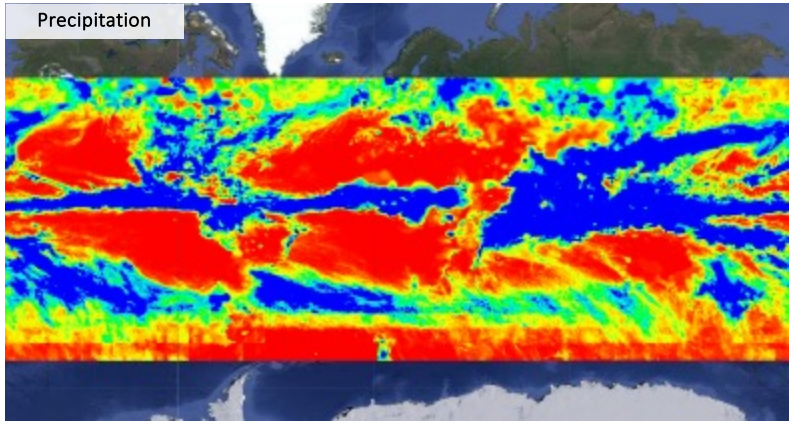

EO data for vegetation monitoring

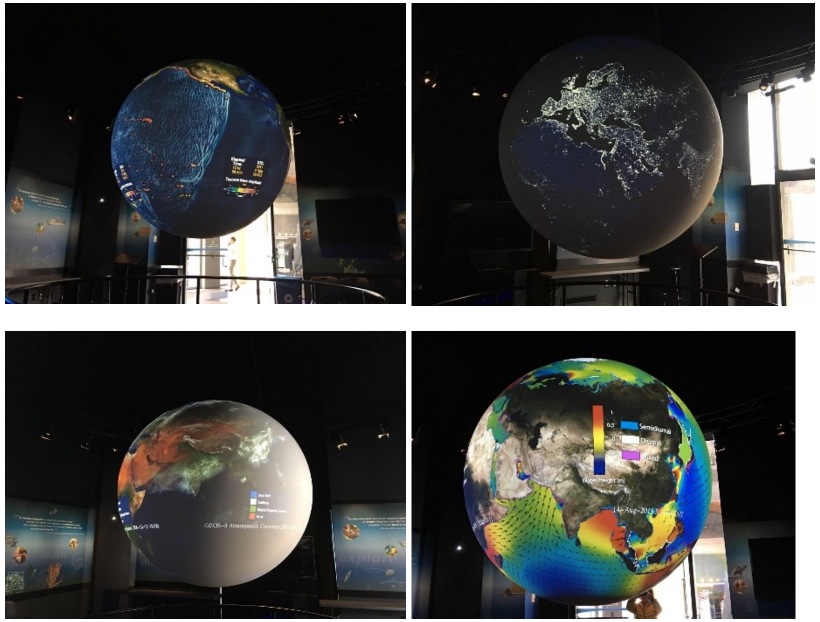

Project’s framework and objectives

- Respond to the need to update and optimize the crop biophysical variable retrieval for agricultural soil and crops using current and present generation EO data considering errors and uncertainties in the remote sensing observations
- Exploit different data processing/assimilation approaches that address the issues of the multi-scale and multivariate nature of the retrieved variables

i) retrieval of crop related bio-physical variables by using RTM, hybrid and empirical models to simulate the interaction of light with vegetation at leaf and canopy levels;

ii) retrieval of agricultural topsoil properties (texture and soil constituencies), using multivariate techniques including machine learning approaches;

iii) optimization of data assimilation procedures of the multivariate and multi-scale remotely sensed variables into agricultural models for yield, quality and biotic & abiotic disease estimation;

iv) development of innovative methods for crop pests and diseases monitoring at the regional scale, with two typical diseases and pests in winter wheat, e.g. stripe rust and powdery mildew, as examples;

v) evaluation of parameters potentially predisposing the onset of pests and diseases;

vi) exploitation of the DIAS systems.

EO Data Delivery

Data access (list all missions and issues if any). NB. in the tables please insert cumulative figures (since July 2020) for no. of scenes of high bit rate data (e.g. S1 100 scenes). If data delivery is low bit rate by ftp, insert "ftp"

ESA /Copernicus Missions	No. Scenes
1.Sentinel-1	20
2.Sentinel-2	300
Total:	320
Issues: China and EU sites	

ESA Third Party Missions	No. Scenes
1.Landsat-8	25
2.MODIS	30
3.Planet	20
4. PRISMA	50
5. ENMAP	3
Total:	128
Issues: both China and EU	

Chinese EO data	No. Scenes
1.GF-1	50
2.GF-2	55
3.GF-6	60
4.ZY-3	20
5.FY	50
Total:	235
Issues: mostly on China and worldwide	

Training of Young Scientists

Name	Institution	Poster title	Level
Zhenhai Li	Shandong University of Science and Technology	Reflections and Applications of Hierarchical Modeling in Agricultural Remote Sensing	Young scientists
Jing Guo	Aerospace Information Research Institute, Chinese Academy of Science	Spatiotemporal Distribution And Main Influence Factors Of Grasshopper Potential Habitat In Two Types Of Steppes In Inner Mongolia, China	Doctor
Hao Yang	Beijing Academy of Agriculture and Forestry Sciences		Young scientists
Linyi Liu	Aerospace Information Research Institute, Chinese Academy of Science		Young scientists
Yu Zhao	Beijing Academy of Agriculture and Forestry Sciences		Young scientists
Dong Han	Beijing Academy of Agriculture and Forestry Sciences		Young scientists
Lei Lei	Beijing Academy of Agriculture and Forestry Sciences		Doctor
Ruiqi Sun	Aerospace Information Research Institute, Chinese Academy of Science		Master

European Young scientists contributions in Dragon 5

Name	Institution	Poster title	Contribution including period of research
Francesco Rossi	University of Rome “La Sapienza” Participated by CNR IMAA	*A Study On The Effects Of Viewing Angle And Solar Geometry Variation In Crop EO Observation.*	Data pre-processing including BRDF model. Crop biophysical vegetation parameter and soil (texture and constituencies) retrieval parameter via MLR and hybrid methods
Simone Saquella	University of Rome “La Sapienza”	Not funded by Dragon 5	Crop mapping, monitoring and algorithm development for pests and diseases detection.
Saham Mirzaei	CNR IMAA	Not funded by Dragon 5	Classification hyperspectral data for crop mapping, spectral indices for biophysical crop parameter retrieval (pigments, proteins)

Setting of Project Research Content

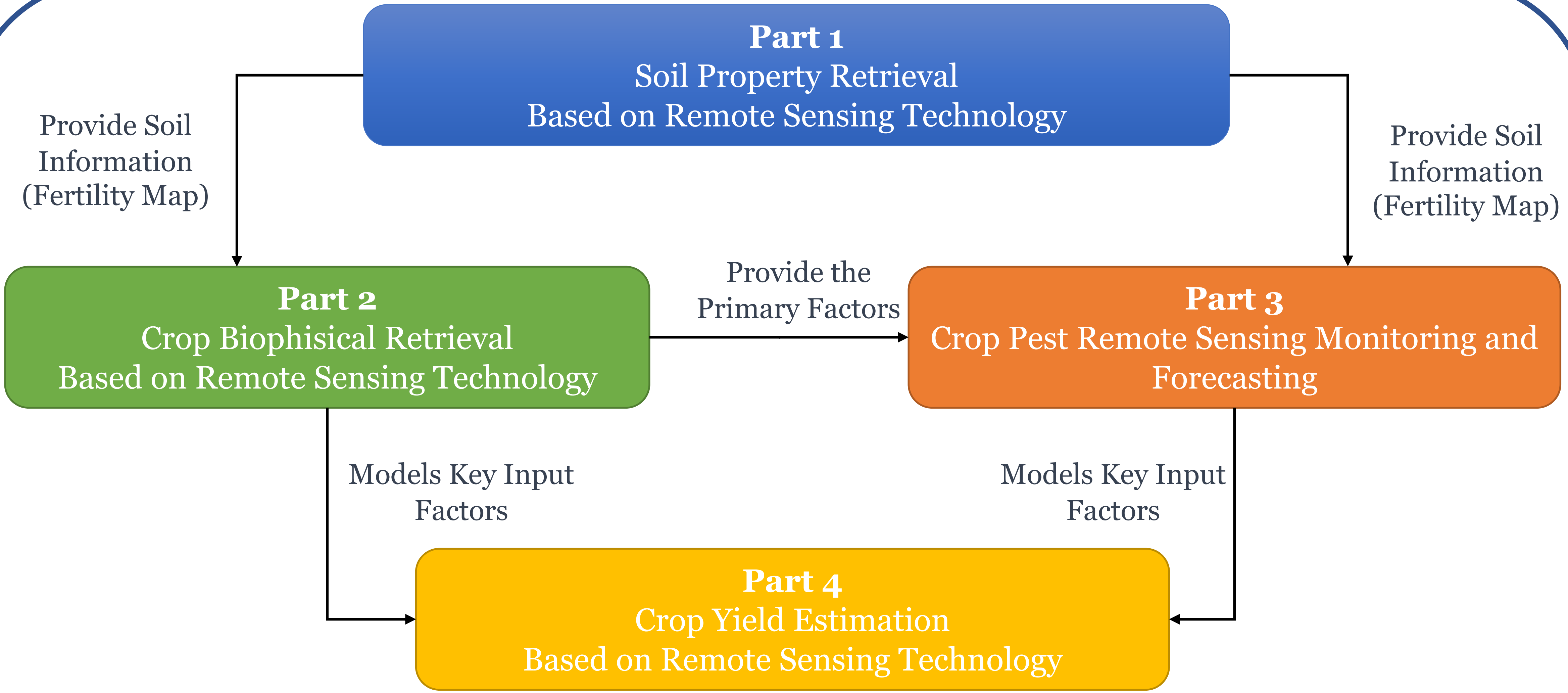

Research Progress

1. **Crop monitoring**
   - Topsoil Characterization
   - Crop Biophysical Parameters Retrieval
   - Crop Yield Estimation
2. Pest and diseases Monitoring and Forecasting
   - Pest (Locust and Grasshopper)
   - Diseases (Yellow Rust)
3. Products and Application

Topsoil Characterization

With the launch of the next generation of hyperspectral satellite sensors in the next years, a high potential to meet the demand for global soil mapping (soil fertility map) and monitoring is appearing.

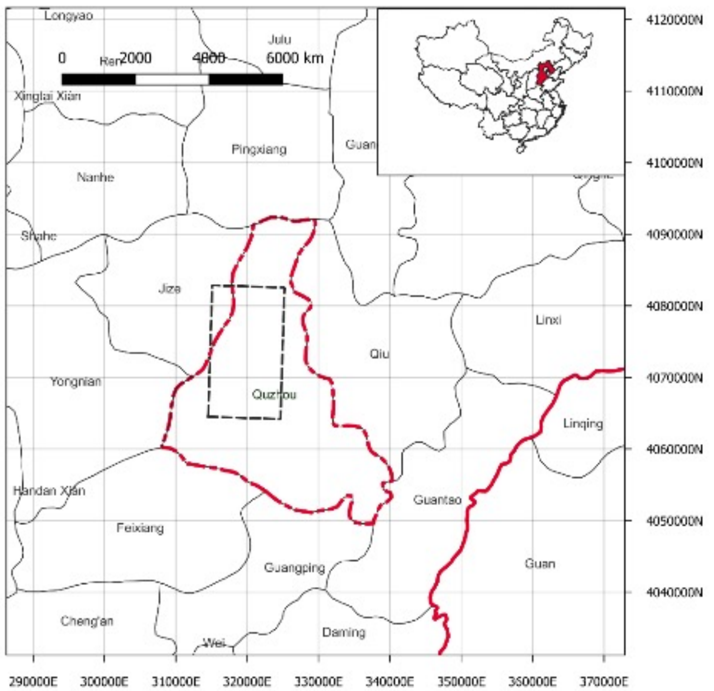

Survey content
PH
Total Nitrogen (%)
Organic Matter (%)
Soil Organic Matter (g/kg)
Soil Nitrogen Content (g/kg)
Effective Phosphorus (g/kg)
Available Potassium (mg/kg)

Quzhou County in the northeast of China.

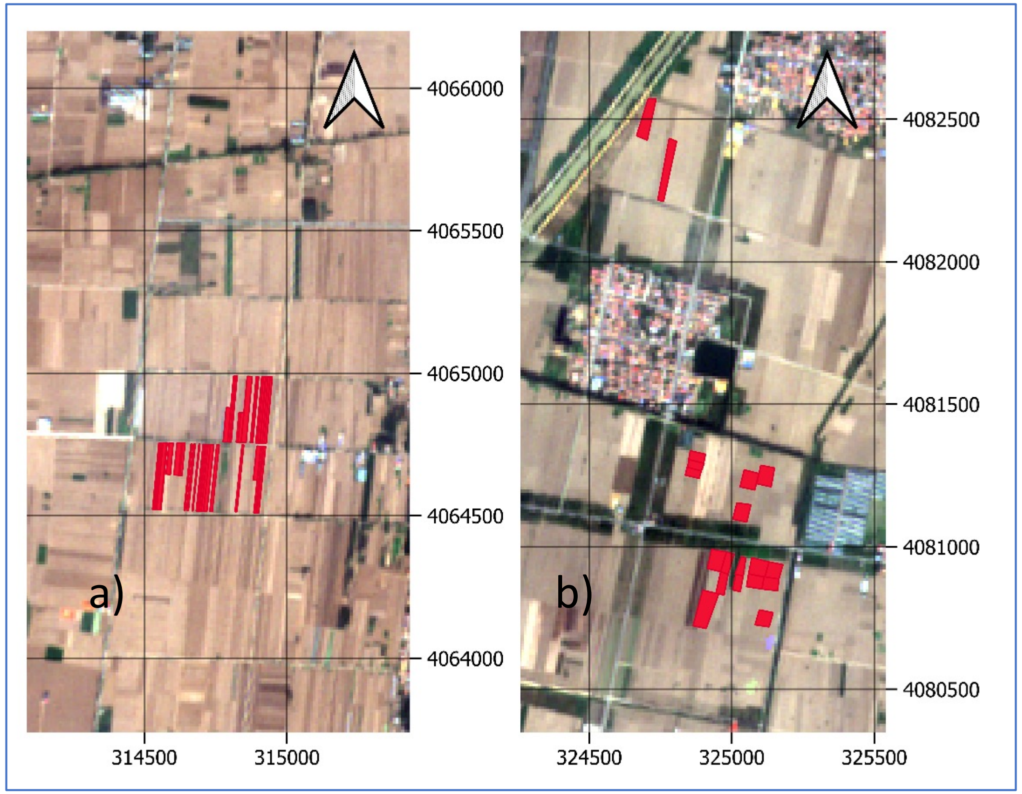

Red Polygons (50) of the study fields.
(a) Fields in the South-West corner of the study area
(b) fields in the North-East corner.
Data source Sentinel-2 19-OCT-2020 RGB image.

Topsoil Characterization

The topsoil properties were investigated using a five-point sampling method, and for each sampling area the specific sampling locations are shown below.

- First remove any plants, stones, etc. from the surface of the soil and dig out small pits using tools.
- Take an appropriate amount of top soil along the cut surface from the bottom upwards, to a depth of approximately 20cm
- The soil obtained from the five points was mixed well, placed in plastic bags and sent to the laboratory for testing

Survey content
PH
Total Nitrogen (%)
Organic Matter (%)
Soil Organic Matter (g/kg)
Soil Nitrogen Content (g/kg)
Effective Phosphorus (g/kg)
Available Potassium (mg/kg)

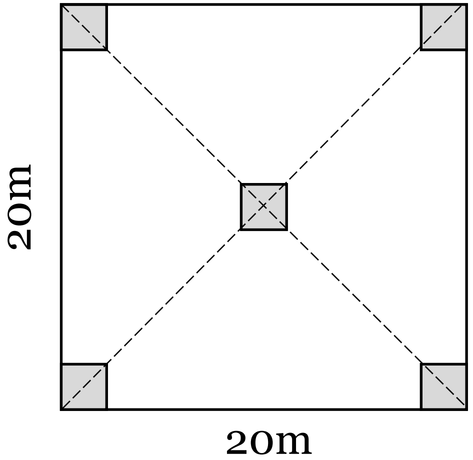

	2019					2020				
	OM (%)	TN (g/kg)	AP (mg/kg)	AK (mg/kg)	pH (-)	OM (%)	TN (g/kg)	AP (mg/kg)	AK (mg/kg)	pH (-)
Min	1.18	0.71	4.87	85.00	7.71	1.12	0.86	5.43	62.00	7.54
Max	2.46	1.44	36.33	318.00	8.17	2.75	1.56	74.20	243.00	8.17
Mean	1.81	1.03	15.68	138.40	7.91	1.86	1.16	18.66	121.53	7.96
Std	0.23	0.14	7.74	46.64	0.10	0.43	0.20	12.12	46.91	0.12

Topsoil Characterization Data Flow

Bare Soil spectra recognition

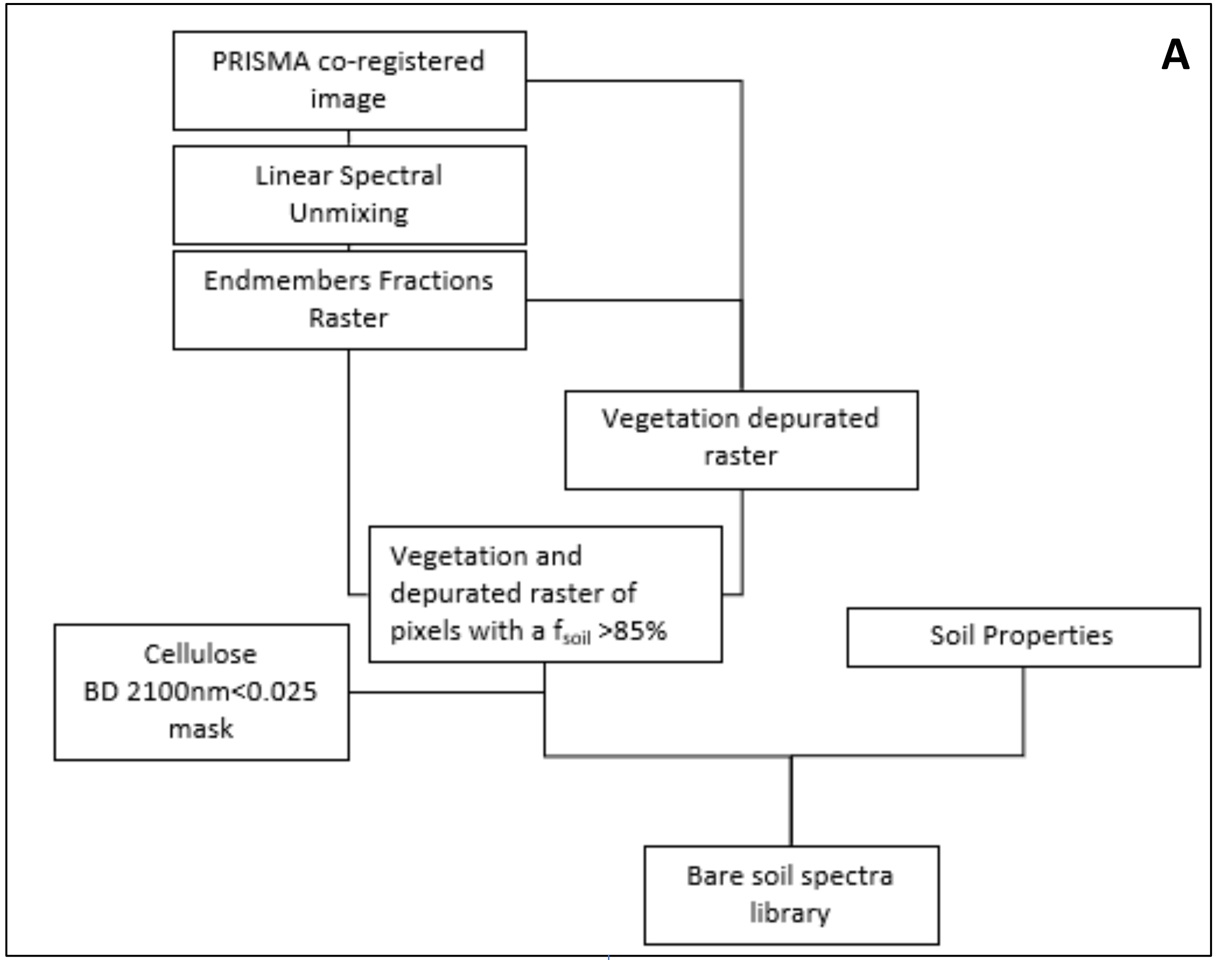

Data spectral pre-treatment

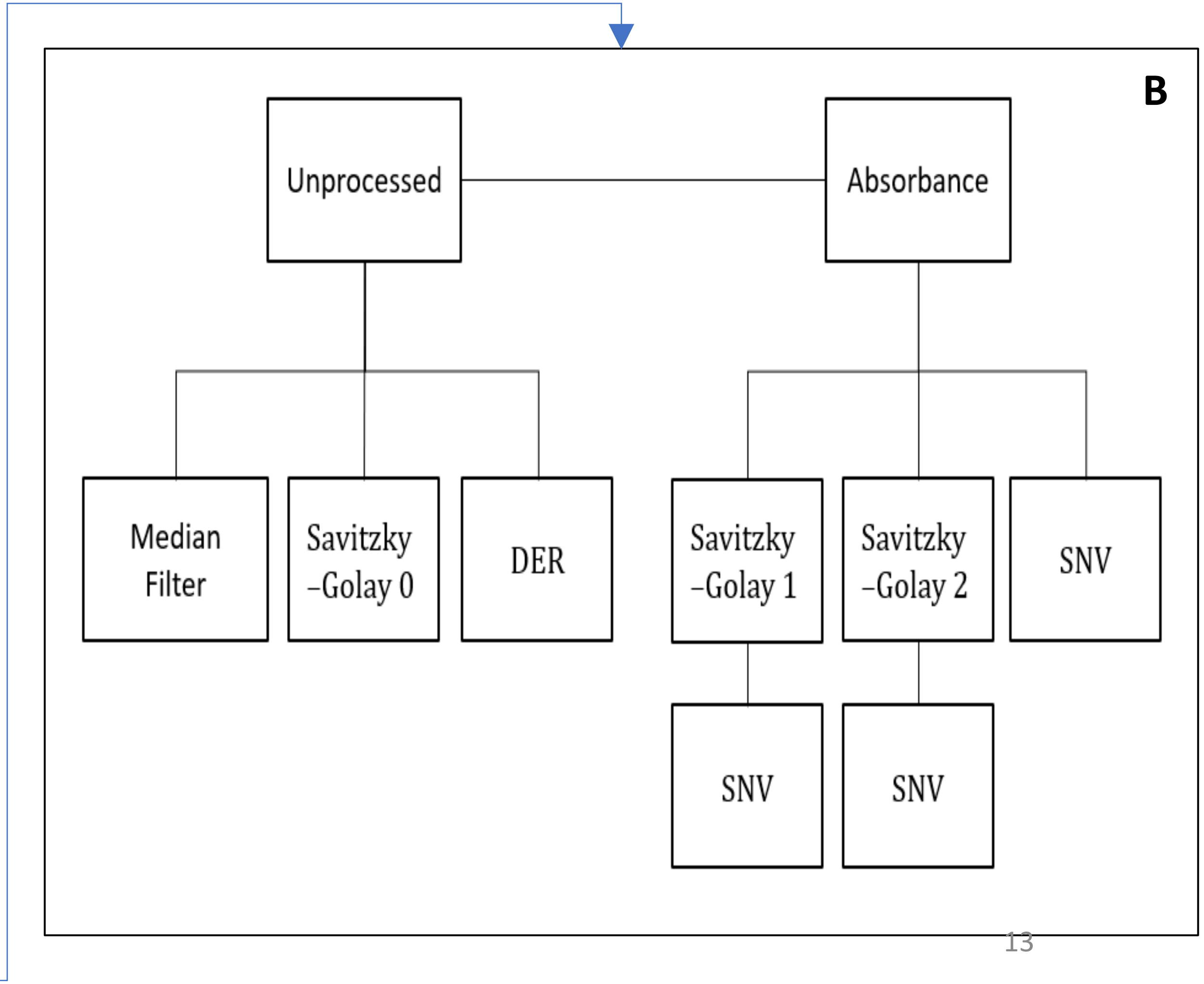

Data Flow MLR algorithms tested

Many methods for applying data-mining approach to soil spectral information have been used and developed, from multiple linear regression (**MLR**) analysis (of the spectra against the chemical/physical data) through principal component analysis regression, partial least squares regression (**PLSR**), artificial neural networks (**ANN**) and random forest among others.

Group	Machine Learning Retrieval Algorithm
Linear Models	Least Squares Linear Regression
	Partial Least Squares Regression
	Regularized Least-Squares Regression
	Principal Components Regression
	Elastic Net Regression
Splines and Polynomials	Adaptive Regression Splines
Tree Models	Bagging trees
	Random Forest
	Canonical Correlation Forests
Kernel Methods	Support Vector Regression
	Kernel Ridge Regression
Gaussian Processes	Gaussian Processes Regression

Data Flow bare soil pixel selection

Explore the synergic use of the constrained Linear Mixing Model (LMM) to separate bare soil and green vegetation (PV) and NPV by the cellulose BD @ 2100nm.

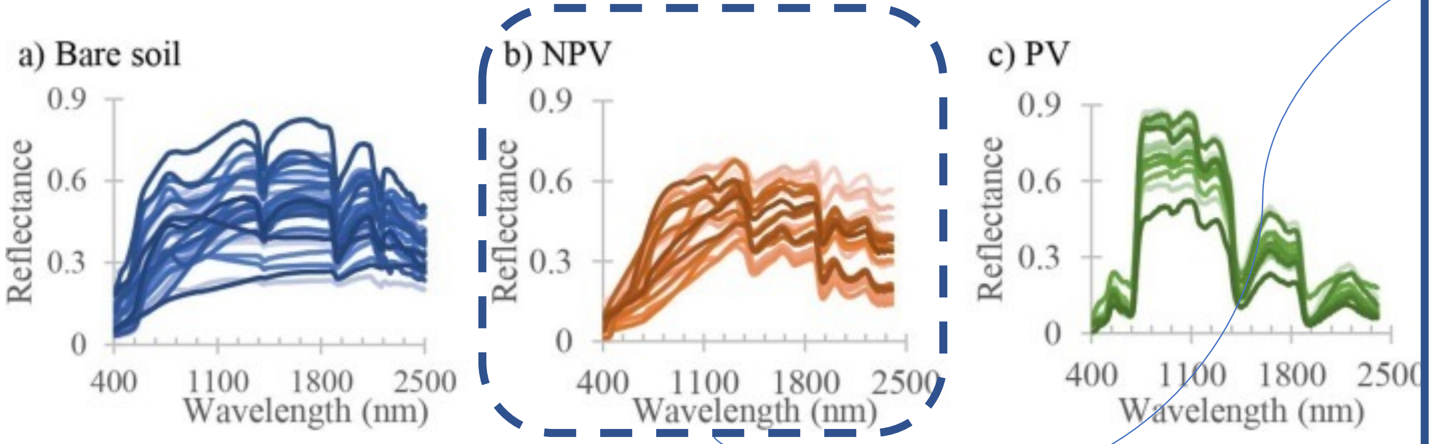

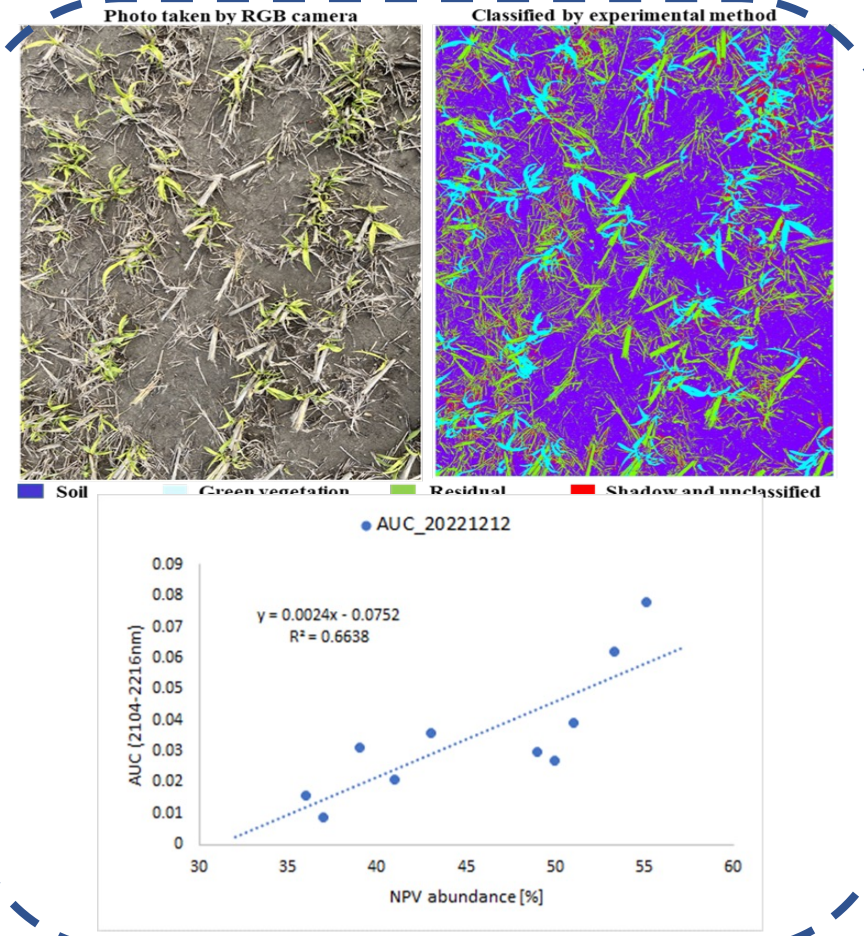

$$R_{TOT} = f_{veg}R_{veg} + f_{soil}R_{soil}$$

$$R_{soil} = \frac{R_{TOT} - (1 - f_{soil}) \cdot R_{veg}}{f_{soil}}$$

The threshold value for f_{soil} of 85% was selected to do not:
(a) exclude an excessive number of pixels
(b) take pixels with a high unmixing RMSE

Data Flow bare soil pixel selection

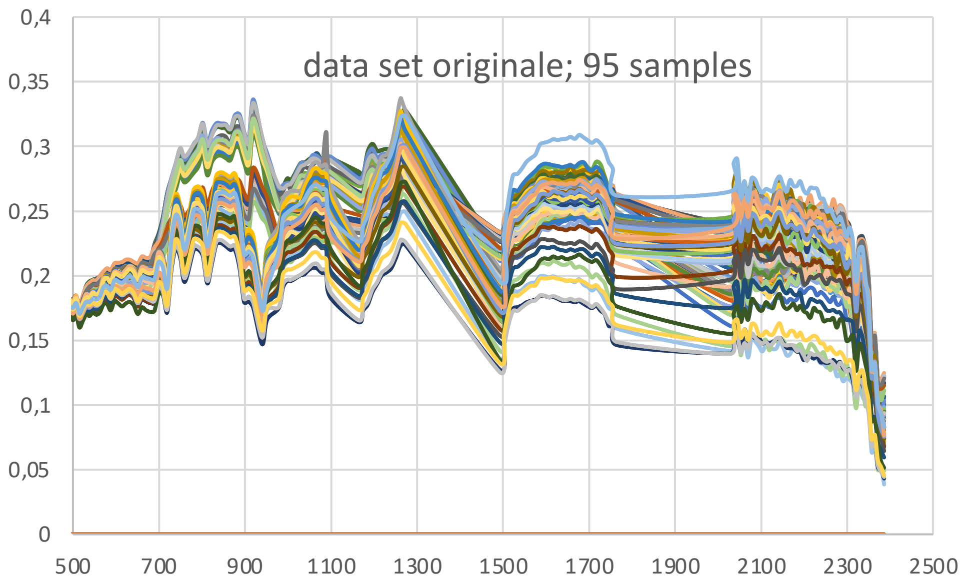

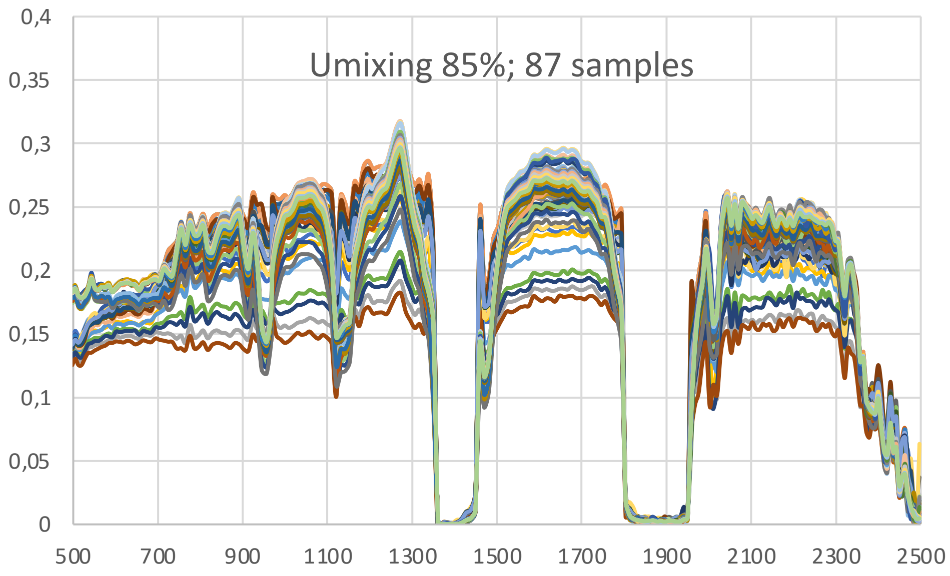

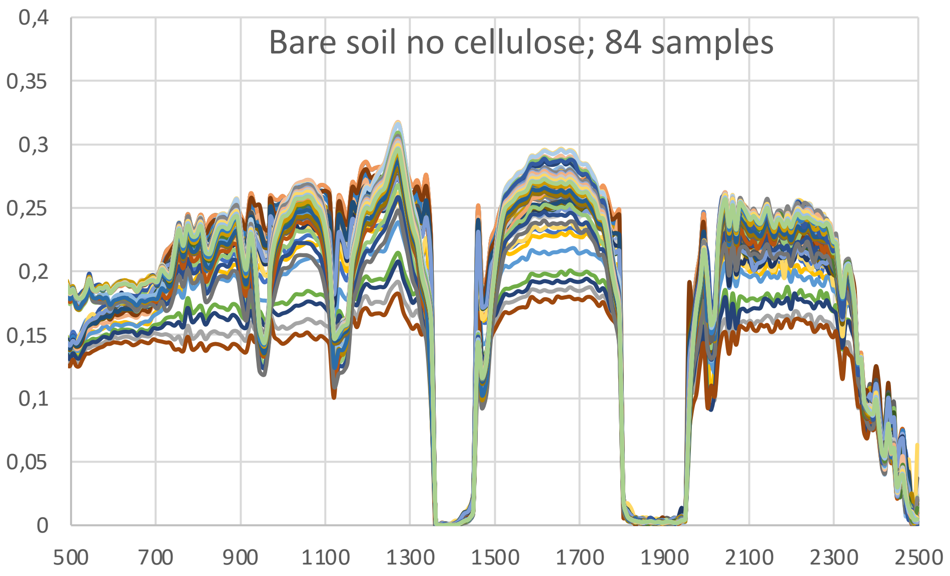

Data Flow MLR algorithms tested

PRISMA	Preprocessing	MLRA	R^2 *Training*	RMSE Test (%)	R^2 Test	RPD	RPIQ
SOC	MF	Support Vector Regression	0.24	0.24	0.39	1.26	1.74
TN	SG2_Abs	Support Vector Regression	0.30	0.13	0.58	1.56	1.57
AP	snv_SG2_abs	Random Forest	0.59	4.70	0.60	1.58	2.26
AK	snv_SG1_abs	Random Forest	0.85	24.59	0.59	1.37	1.66
PH	Untreated	Regularized least-squares regression	0.65	0.07	0.25	1.34	1.82

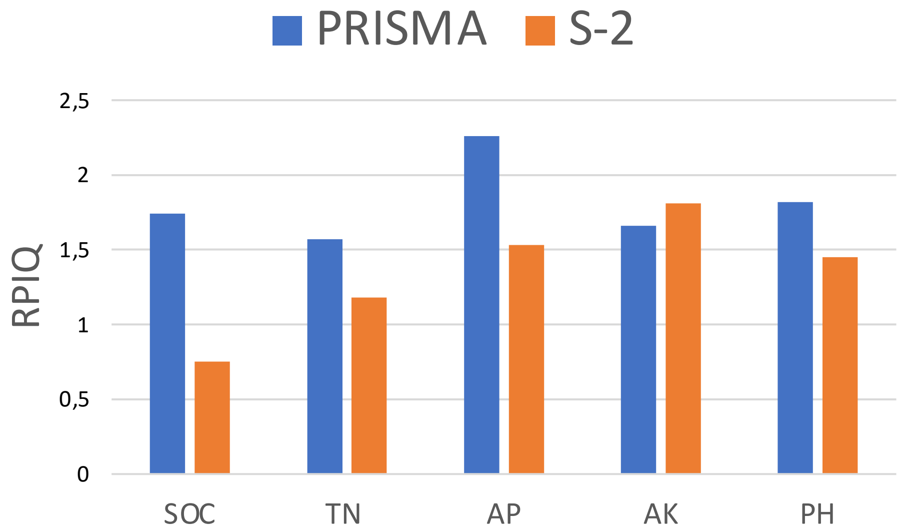

S-2	Preprocessing	MLRA	R^2 *Training*	RMSE Test (%)	R^2 Test	RPD	RPIQ
SOC	S2_Absor	Canonical Correlation Forests	0.92	0.29	0.25	1.18	0.75
TN	S2_Absor	Random Forest (TreeBagger)	0.71	0.16	0.44	1.34	1.18
AP	S2_Refl	Support Vector Regression	0.02	11.34	0.30	1.03	1.53
AK	S2_Absor	Partial least squares regression	0.59	42.60	0.46	1.33	1.81
PH	S2_Refl	Kernel ridge Regression	0.55	0.11	0.23	1.13	1.45

Soil fertility map

Soil constituents' prediction maps obtained applying the best performing MLRA and preprocessing on the PRISMA image of 05-November-2022.

For each subplot on the left are the fields in the South-West corner of the study area and on the right the fields in the North-East corner. Black pixels belong to pixels covered by vegetation and dominant in NPV residues.

The predictions by using PRISMA are better than those obtained by S-2 both in terms of RMSE and RPD.

Organic Matter

Total Nitrogen

Effective Phosphorous

Available Potassium

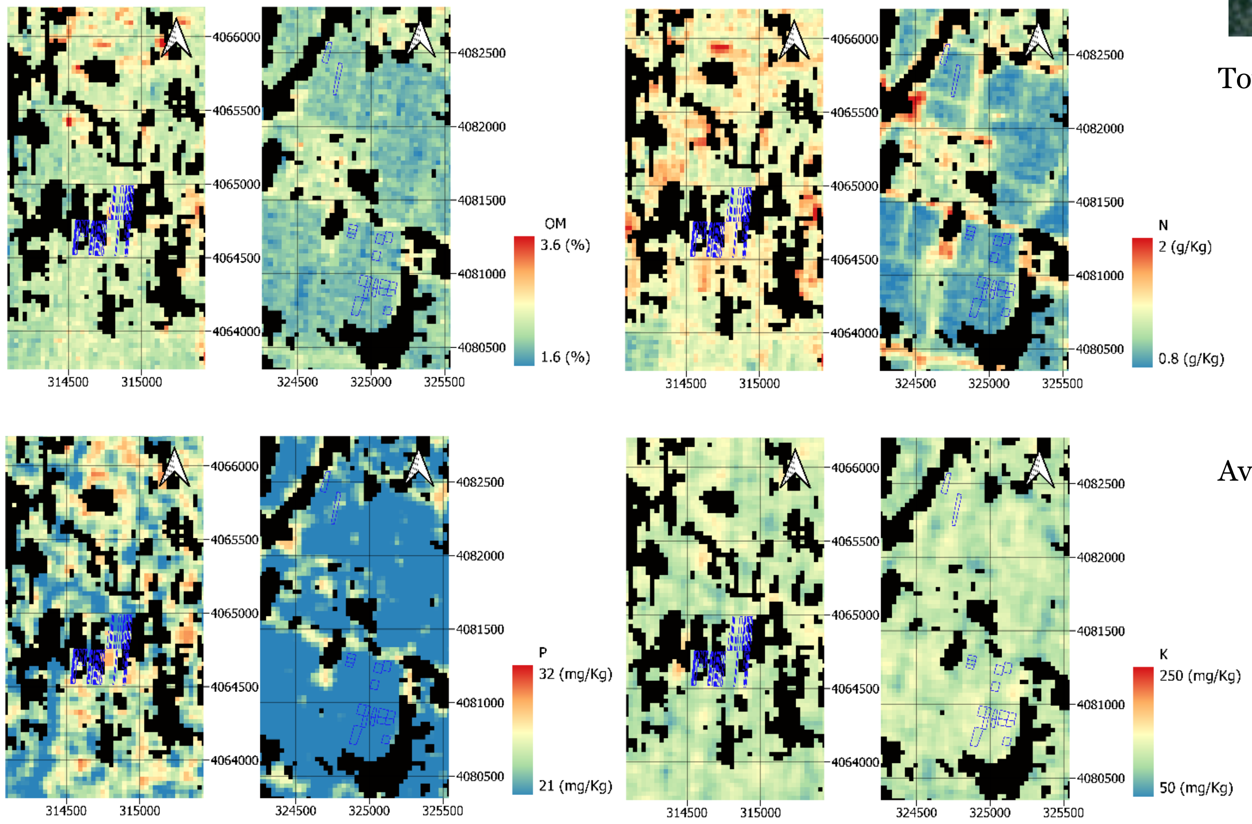

Ph

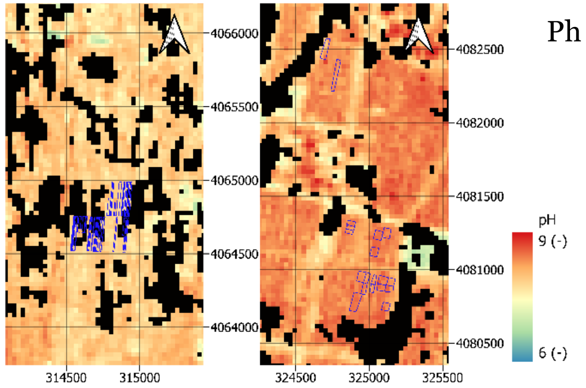

The predicted accuracy for nutrients retrieval in terms of RMSE (24.59 $mgkg^{-1}$ for **P**; 4.70 $mgkg^{-1}$ for **K**) is comparable to the one given by Song et al. 2018 and Yu et al. 2018 on different Chinese test sites using lab spectra

Research Progress

1. Crop monitoring

- Topsoil Characterization
- Crop Biophysical Parameters Retrieval
- Crop Yield Prediction

2. Pest and diseases

- Pest (Locust and Grasshopper Forecasting)
- Diseases (Yellow Rust)

3. Products and Application

Field Data Collection Campaigns – biophysical variables

Canopy Variables:
- LAI
- FCOVER
- FAPAR

Definition of field measurement and sampling methods.

Measurement protocol and validation metrics for crop vegetation

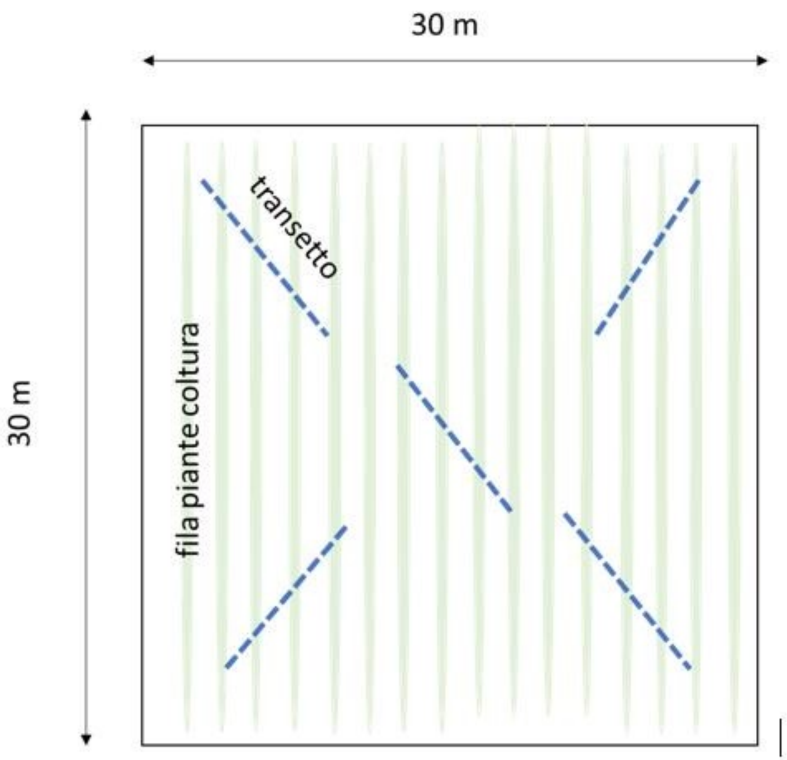

serie A BBBBBBB A (cioè una misura Above + 8 misure Below + 1 misura Above). Impostare Menu > Log Setup > Transcomp > Determine Above > Interpolate.

Se c'è il sole, almeno ogni ora effettuare una serie di misure separate di 4 A per la determinazione di **K** (scattering correction)

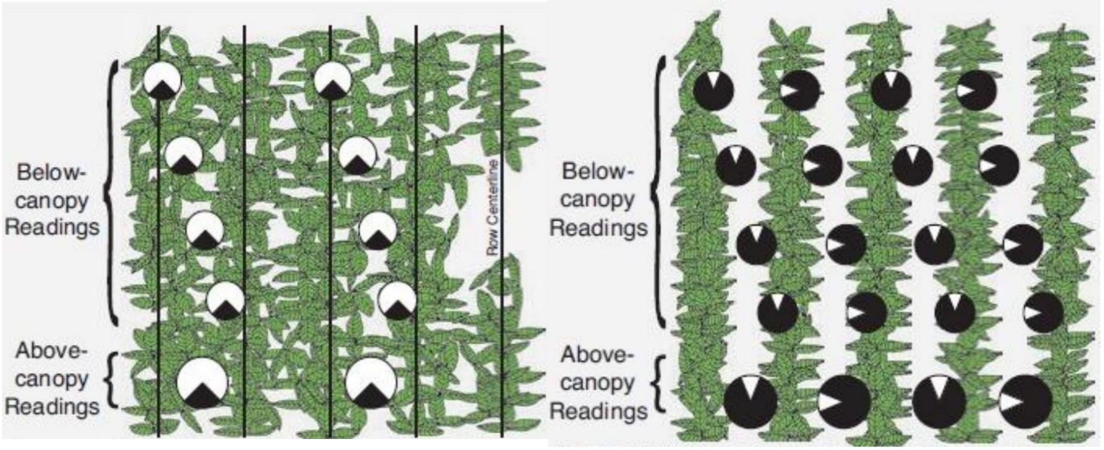

Definition of field measurement and sampling methods.

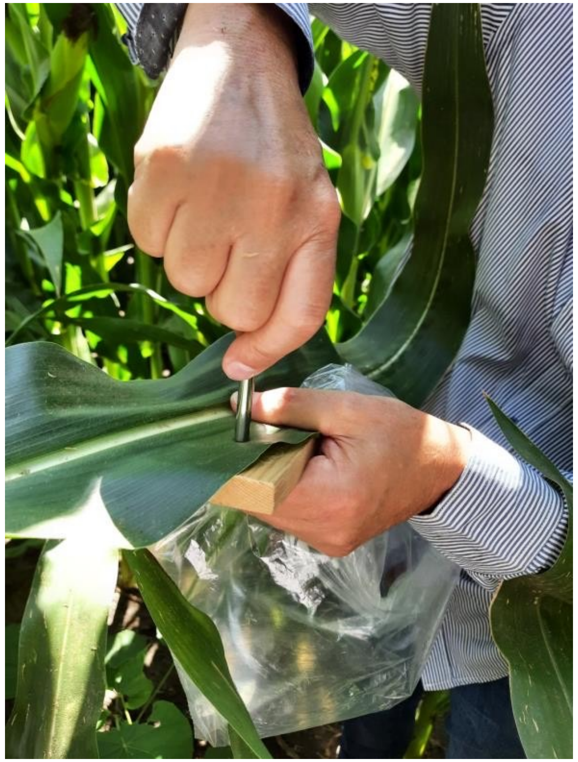

Leaf Variables:
- EWT
- LMA
- N%
- C%
- Cab
- Car

- 12 leaf disks per transect from 4x3 leaves [60 disks per ESU]
  - 50% dried for EWT & LMA
  - 50% frozen – 20°C for Cab & Carotenoids lab analysis

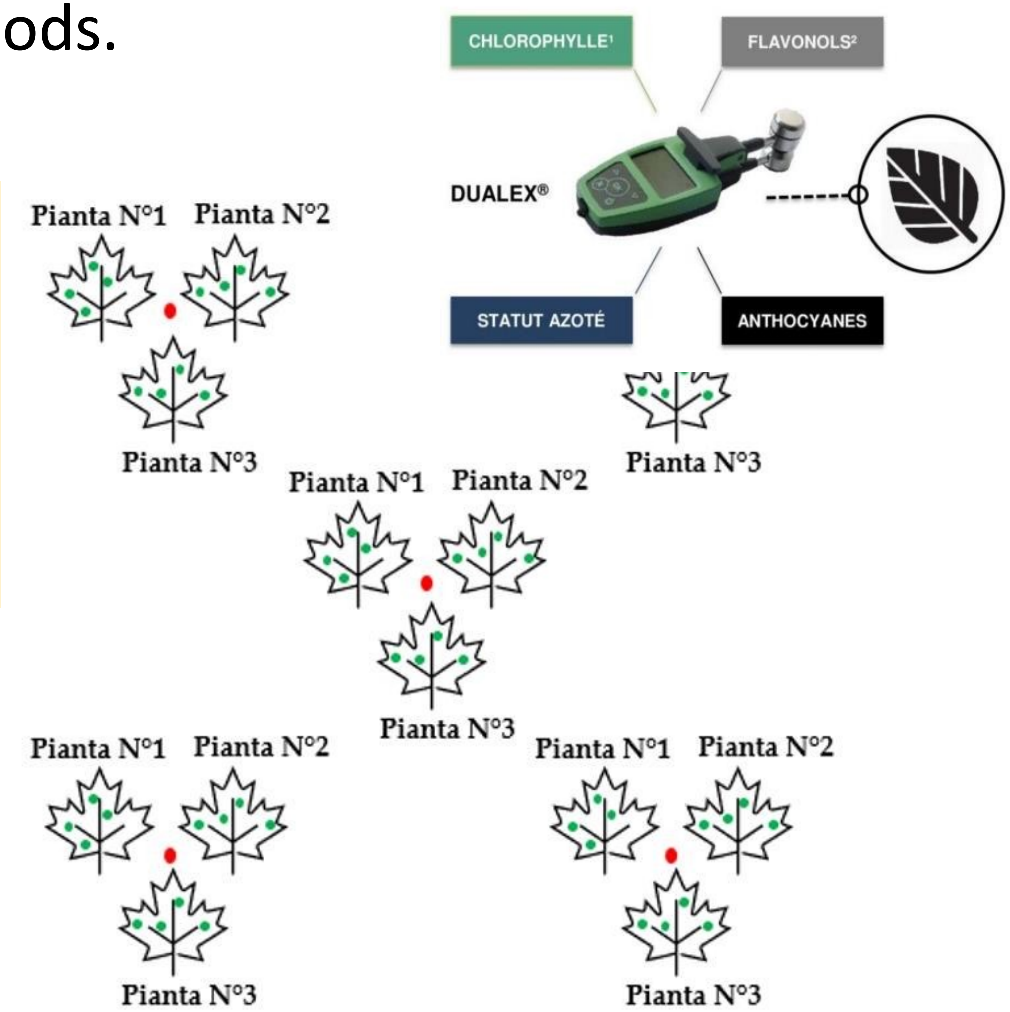

Field Data Collection Campaigns - biophysical variables

Field monitoring campaigns at the Maccarese site (IT): 2022 maize season

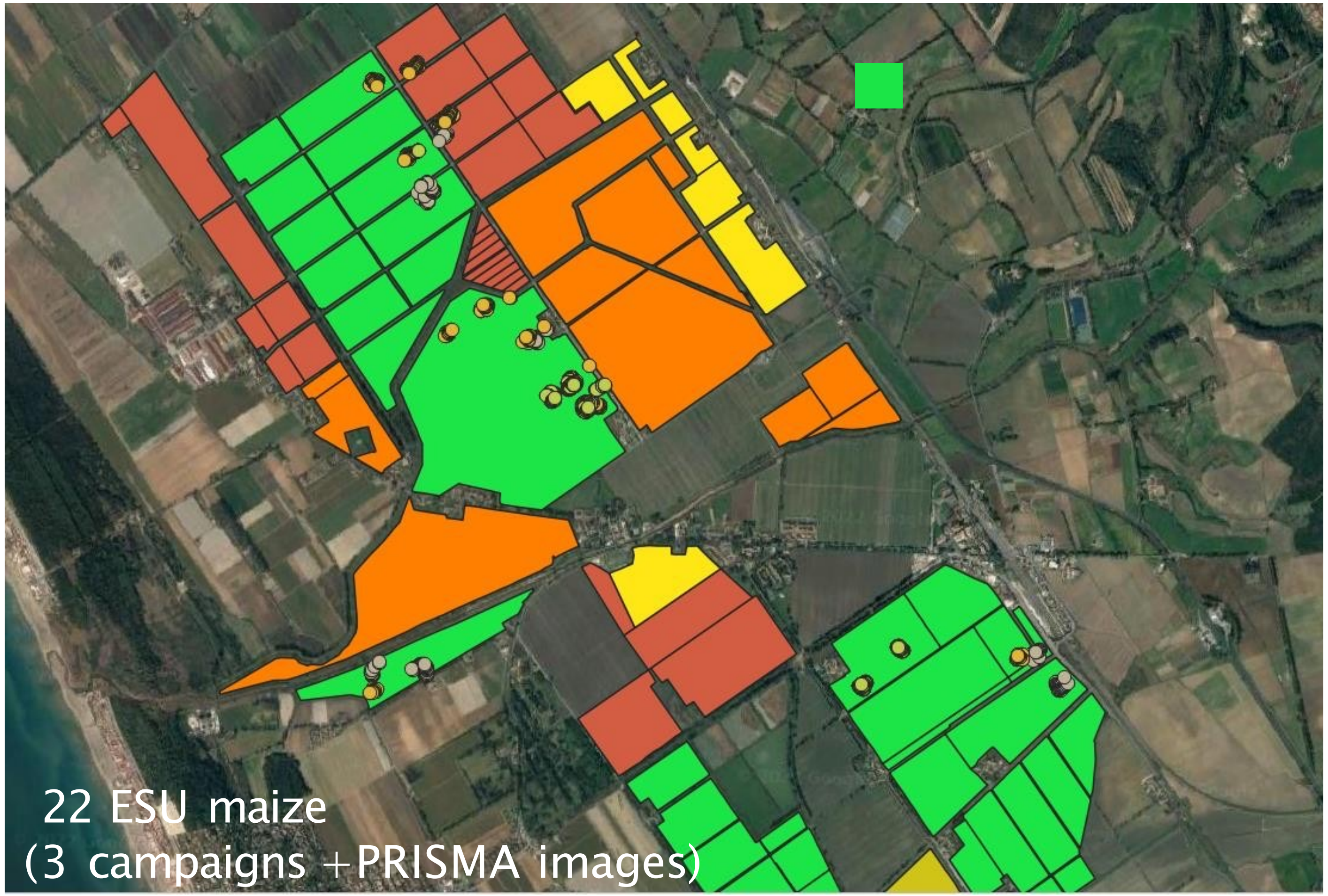

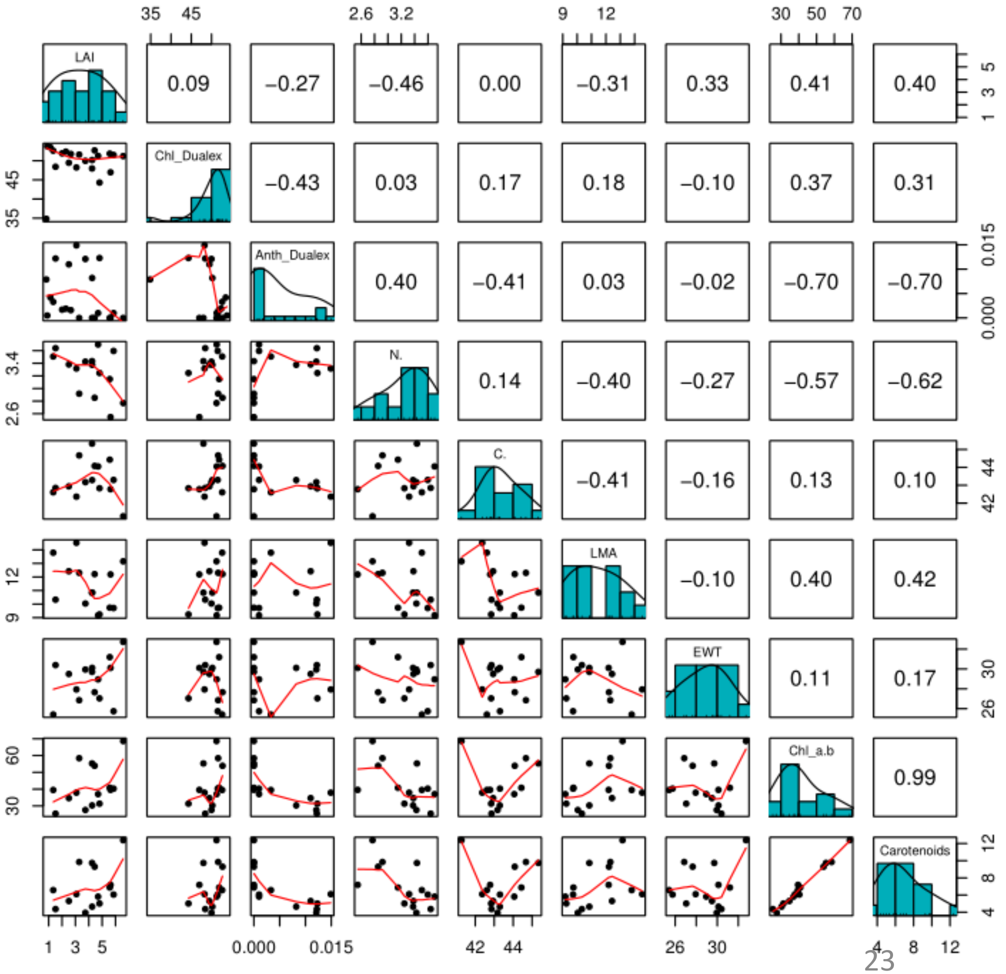

Spectral Algorithm for crop biophysical Retrieval

EWT leaf equivalent water thickness (LEWT) is an important parameter in ecological and environmental monitoring. It applies the Beer-Lambert law to inversely determine (constrained minimization) the optical thickness *d* of the water layer responsible for the water absorption feature at 970 nm

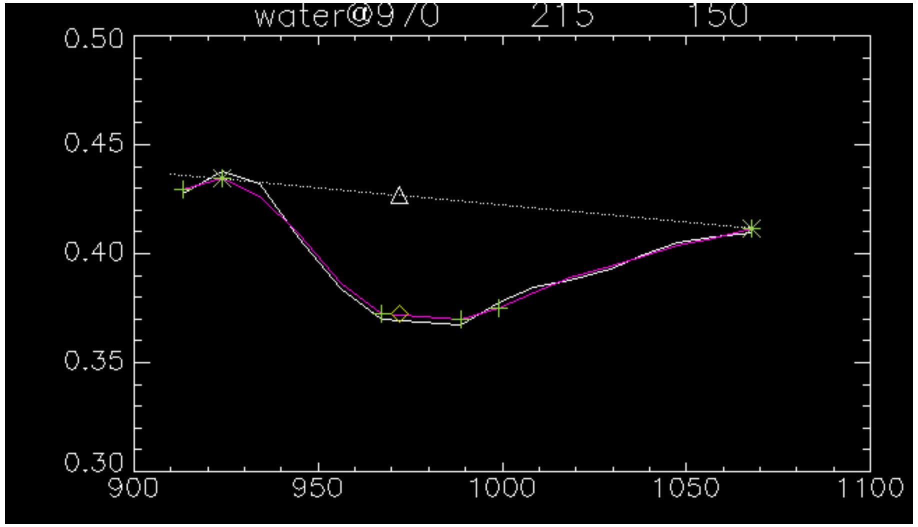

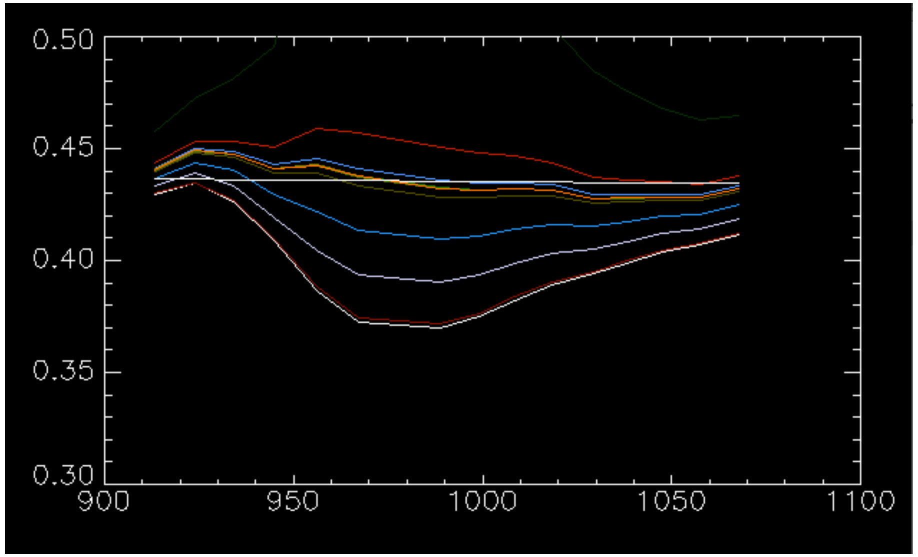

BD = 1 – RC

Gaussian fitting of the 900-1100nm spectra

CW, FWHM

$$R' = \frac{R_0}{e^{-\alpha(\lambda)d}}$$

constrained min
(Generalized Reduced Gradient Method)

Spectral Algorithm for crop biophysical Retrieval

Performance on simulated data

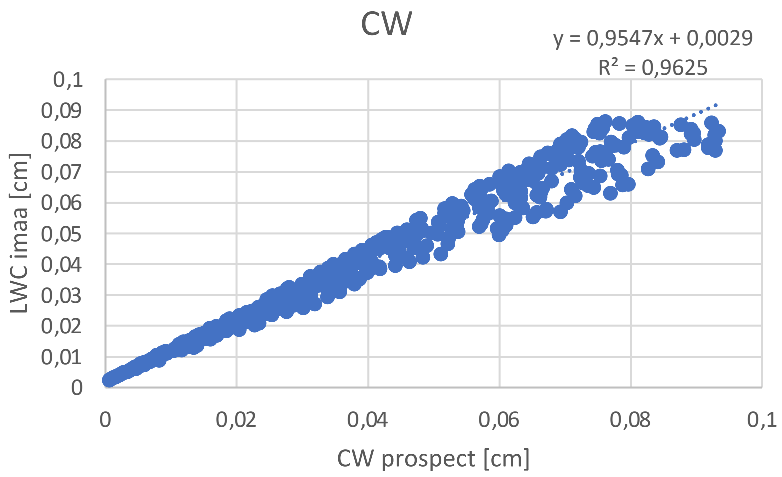

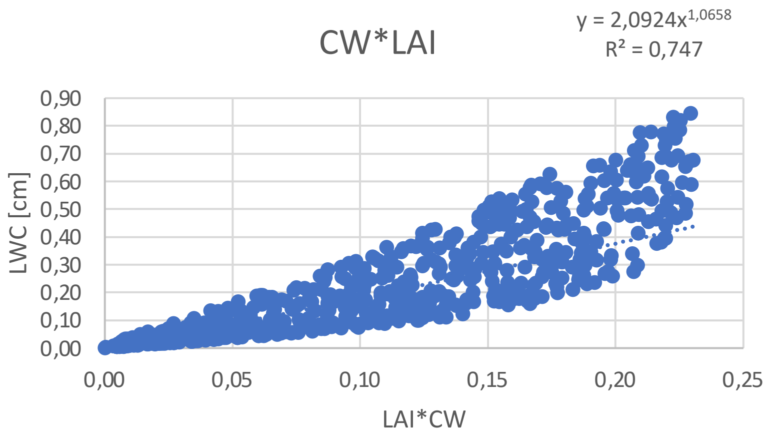

Validation on real hyperspectral (PRISMA) data

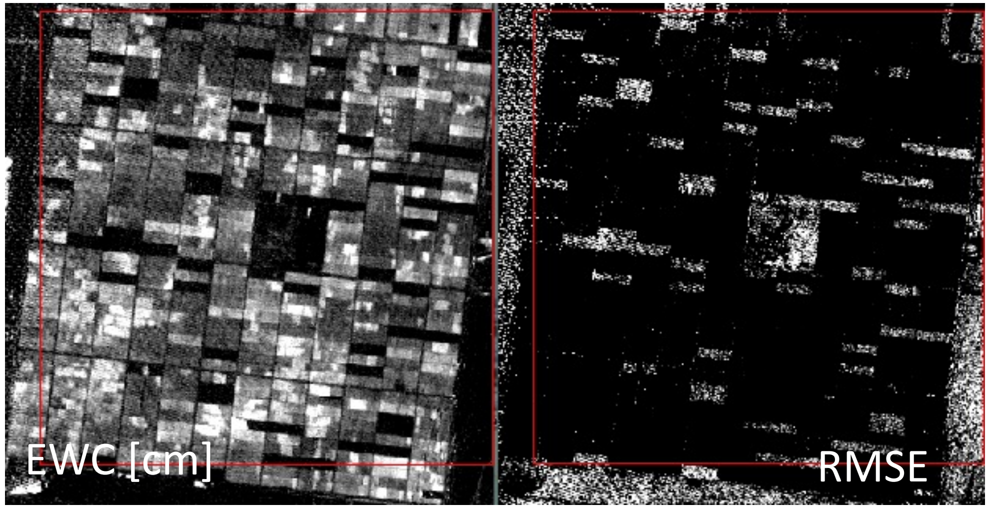

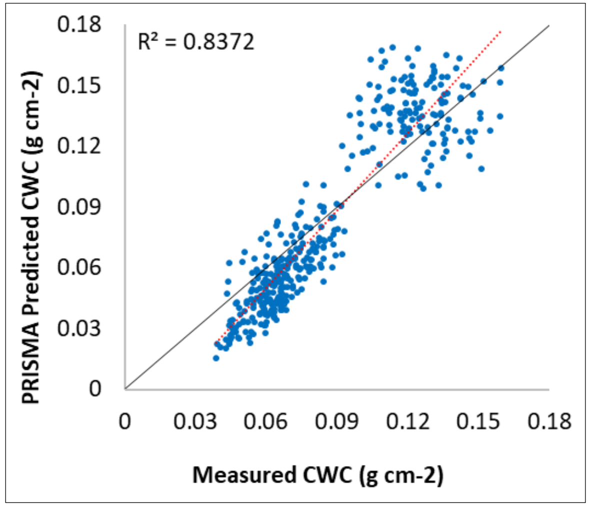

The external validation performed on middle East sugarcane data

Hybrid methods for biophysical variables retrieval

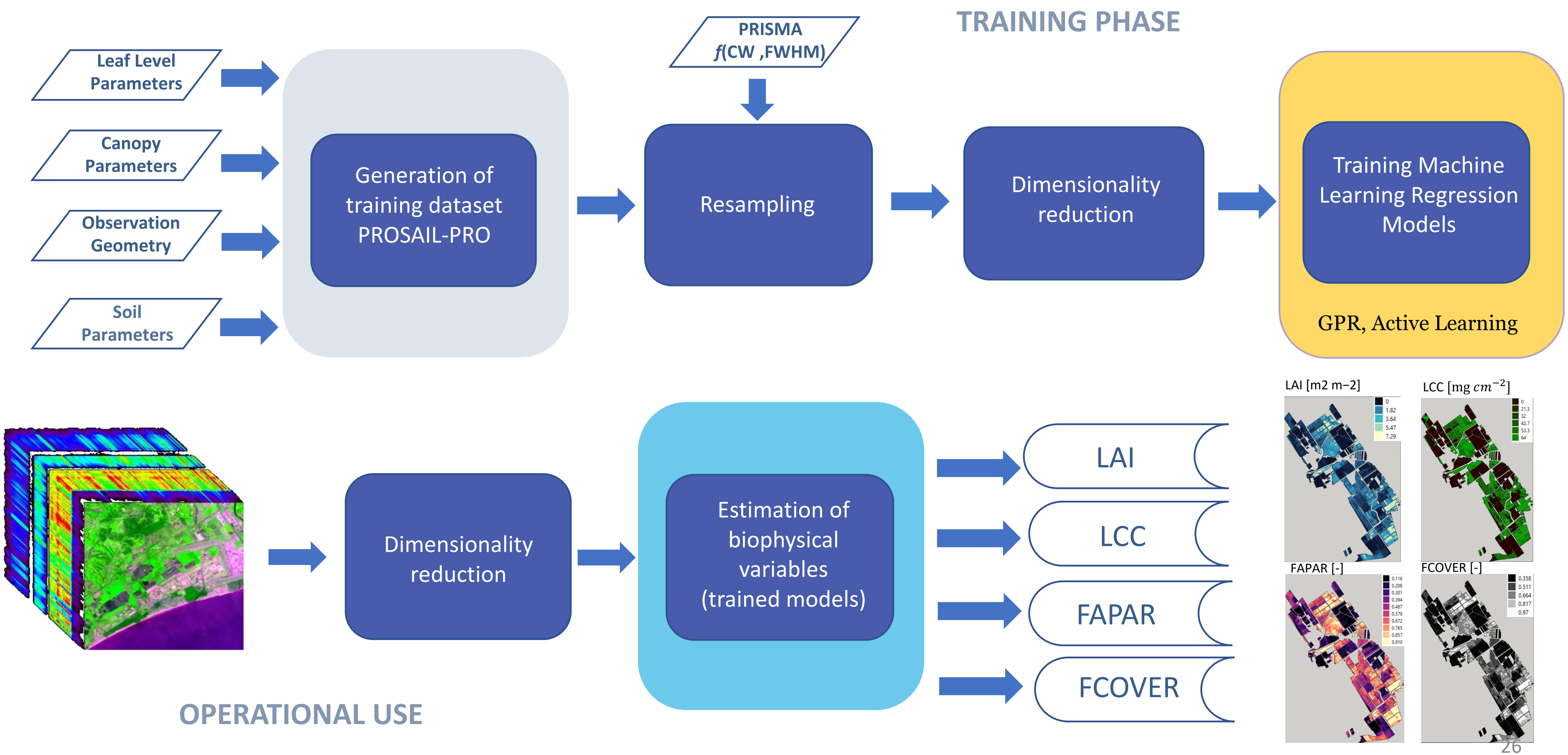

Hybrid methods for biophysical variables retrieval

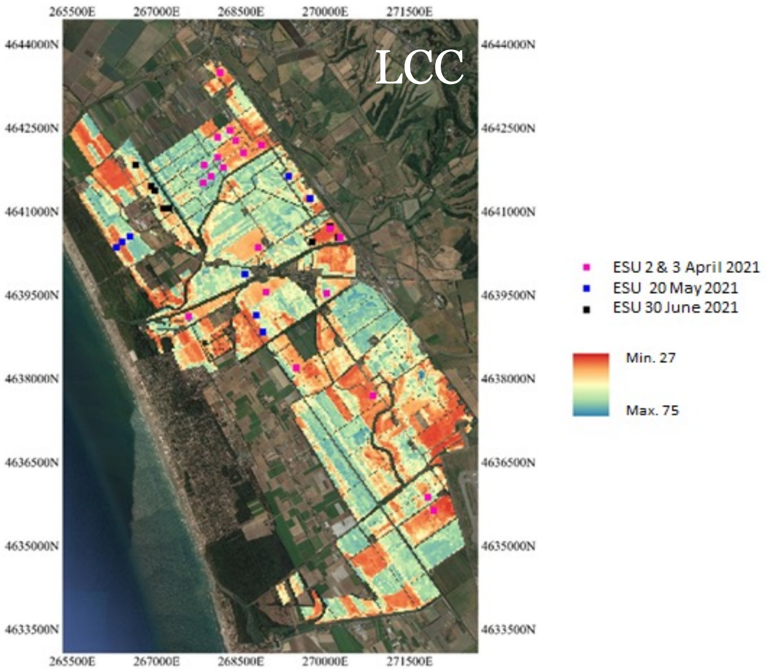

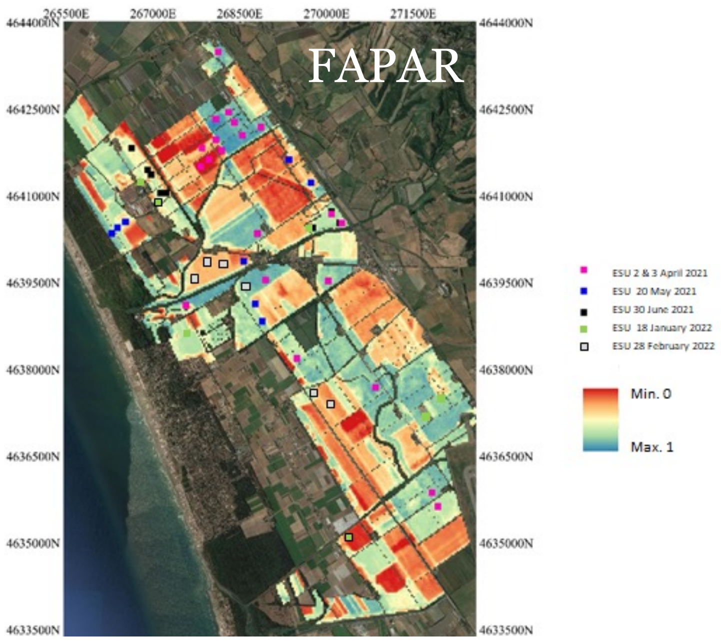

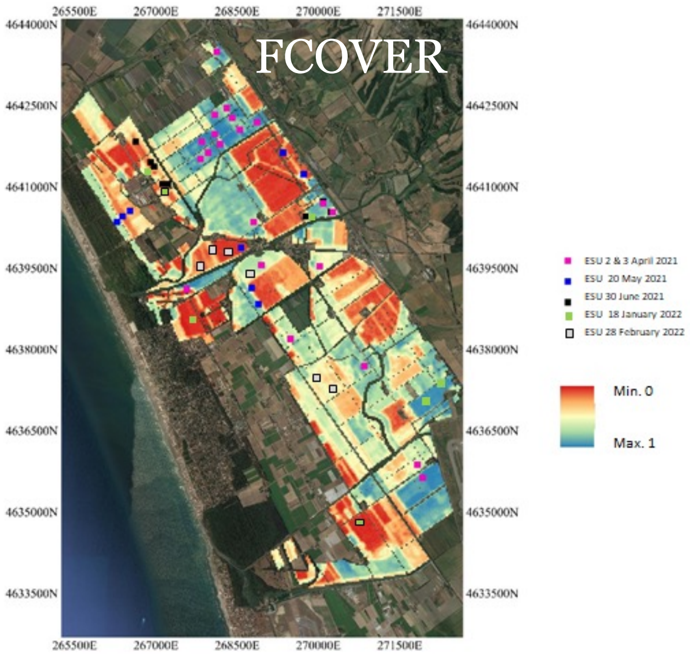

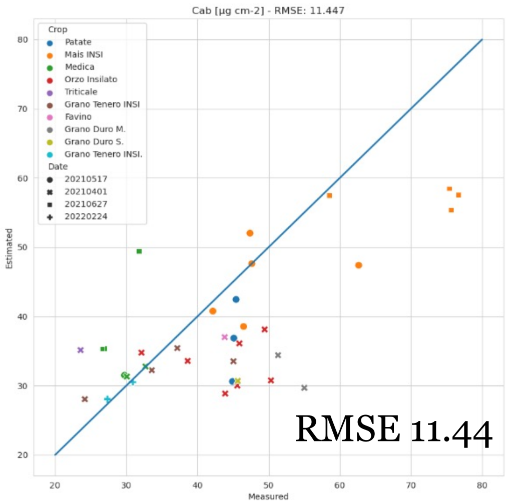

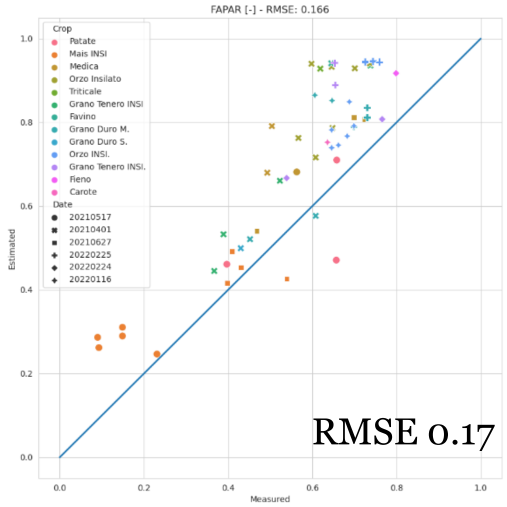

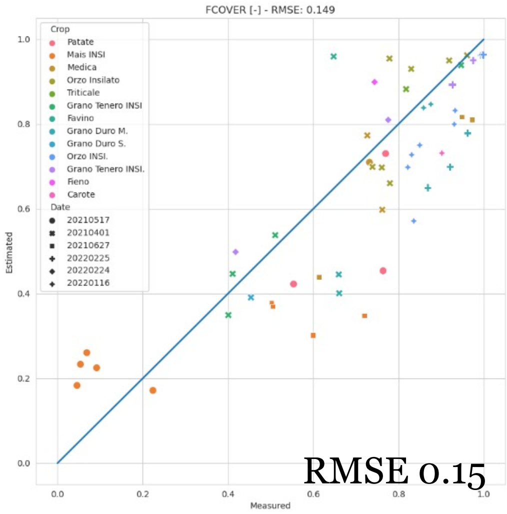

Hyperspectral vs Multispectral

PRISMA	BIAS	RMSE	RRMSE	MAD	R^2	Pearson	RPD	RPIQ
LAI	0.12 m^2m^{-2}	0.78 $m^2\ m^{-2}$	0.25	0.61 $m^2\ m^{-2}$	0.87	0.93	2.23	2.94
LCC	5.59 $\mu g\ cm^{-2}$	11.45 $\mu g\ cm^{-2}$	0.26	8.99 $\mu g\ cm^{-2}$	0.46	0.68	1.21	1.41
FCOVER	0.06	0,15	0.21	0.12	0.71	0.84	1.72	2.01
FAPAR	-0.14	0.16	0.29	0.15	0.78	0.88	1.06	1.33

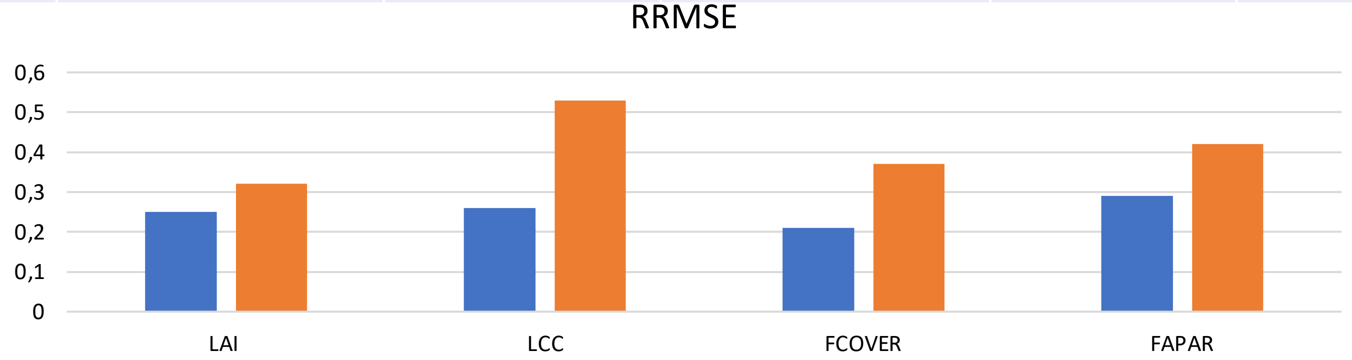

Sentinel-2	BIAS	RMSE	RRMSE	MAD	R^2	Pearson	RPD	RPIQ
LAI	0.44 m^2m^{-2}	0.99 $m^2\ m^{-2}$	0.32	0.78 $m^2\ m^{-2}$	0.78	0.88	1.74	2.3
LCC*	-5.20 $\mu g\ cm^{-2}$	23.25 $\mu g\ cm^{-2}$	0.53	18.75 $\mu g\ cm^{-2}$	0.15	-0. 39	1.21	1.40
FCOVER	0.10	0.25	0.37	0.17	0.43	0.65	1.68	2.00
FAPAR	-0.06	0.23	0.42	0.19	0.46	0.68	1.08	1.35

Crop Biophysical Retrieval Based on Optical and Radar RS data

High-precision remote sensing inversion products of vegetation leaf area index in key regions around the world

- **Take advantage of the high spatial resolution of Sentinel-2 data to improve the spatiotemporal resolution and inversion accuracy of leaf area index products**
- **Establish an inversion model that couples optical and radar data to solve the problem that the inversion accuracy is affected by vegetation canopy characteristics (such as plant shape)**

LAI inversion model combining active and passive methods

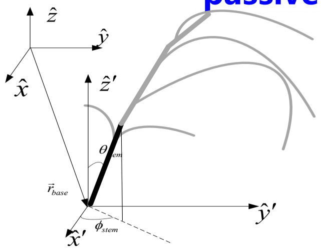

$$RVI_{Freeman} = \frac{P_V}{P_S + P_D + P_V}$$

Radar Vegetation Index

$$LAI = \beta_0 * ALA^{\beta_1} * NDVI^{\beta_2}$$

$$MEVI = RVI_{Freeman} * 2.5 * (R_{Nir} - R_{Red}) / (1 + R_{Nir} + 6 * R_{Red} - 7.5 * R_{Red})$$

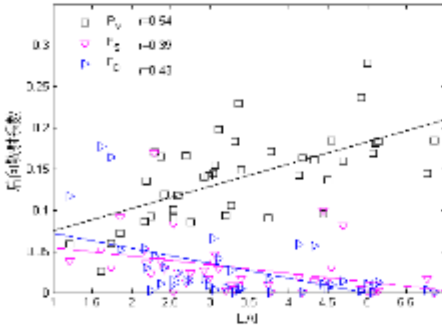

Relationship between backscattering coefficient and LAI

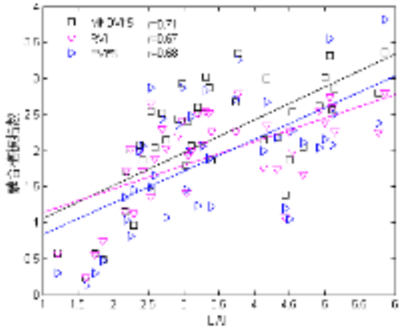

Relationship between Integrated vegetation index and LAI

direct test results

Crops and grasslands in Jiu San Reclamation Area of Heilongjiang, Luohe of Henan, Shunyi of Beijing and Xilingol were selected for verification, and the calculation accuracy was

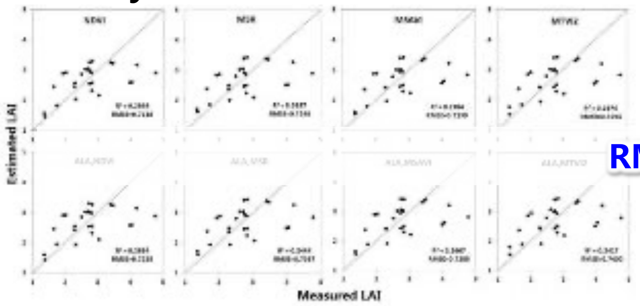

Comparative analysis with MODIS products

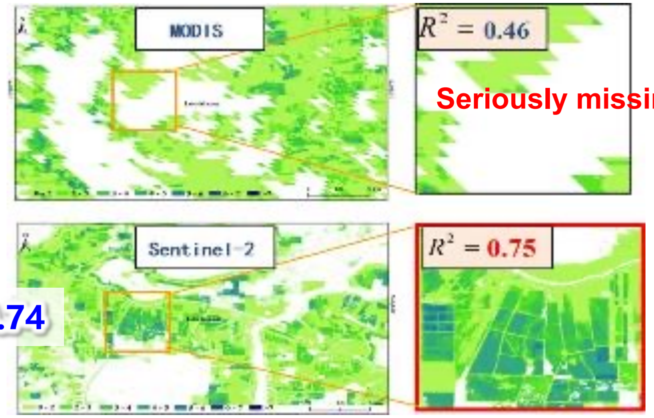

RMSE<0.74

Model advantages:

- **Compared with the traditional single index method, the LAI inversion algorithm based on vegetation-sensitive bands can effectively improve the inversion accuracy, with R^2 up to 0.87 and RMSE<0.74.**
- **Vegetation inversion products based on Sentinel-2 and high-resolution data not only have higher spatial resolution , but also have more complete spatial continuity.**

Crop Biophysical Retrieval Based on MLRA

High-precision remote sensing inversion products of vegetation chlorophyll content in key areas around the world

- Proposed a multi-source high-resolution satellite data fusion scheme to improve the data quality and spatial and temporal resolution of the product ;
- a chlorophyll inversion model for global key areas based on the random forest model (RF) to achieve high-precision dynamic inversion of chlorophyll content and vegetation growth monitoring

Technical plan for chlorophyll content inversion in key regions around the world

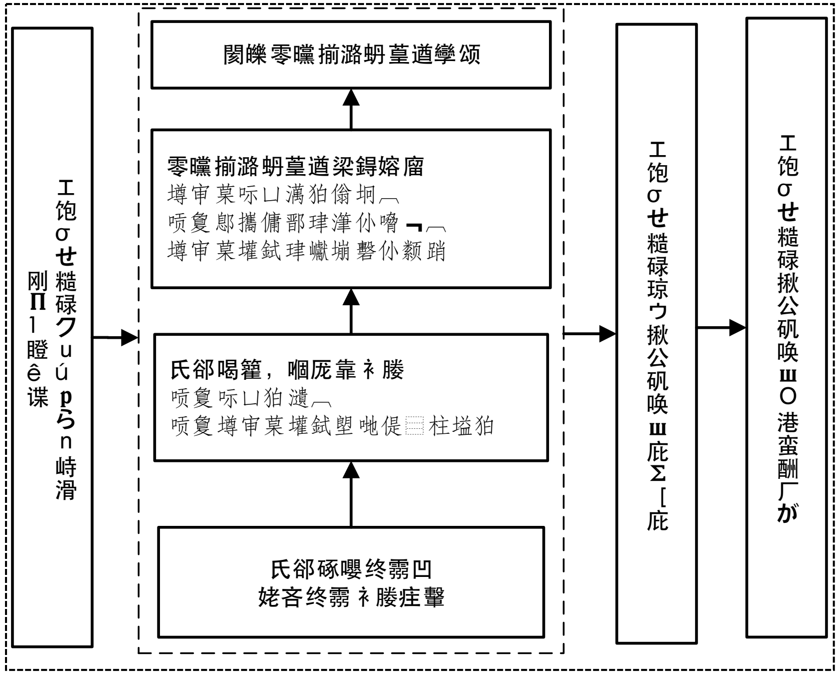

Direct test results: R^2=0.80, RMSE=7.61

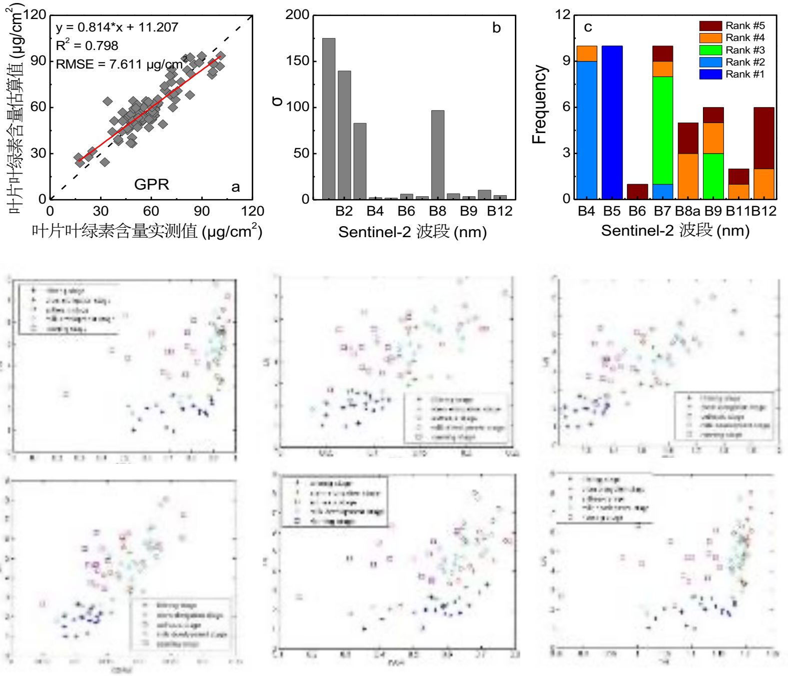

Indirect test results: comparison with MODIS

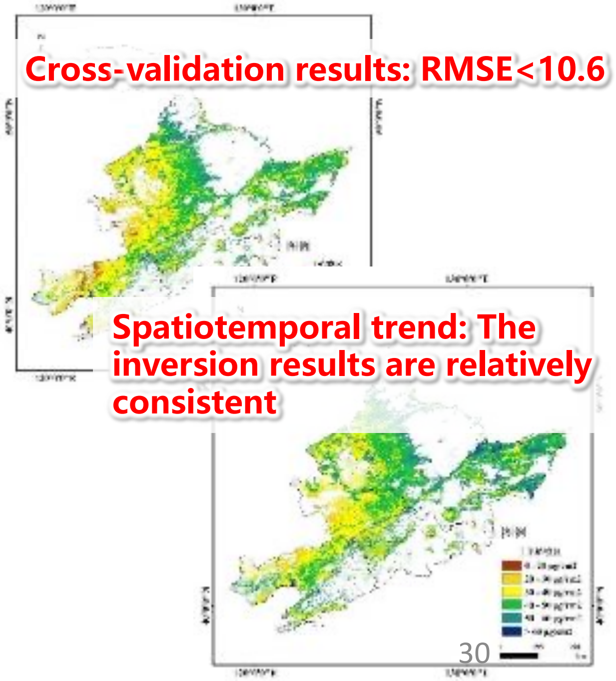

High-precision remote sensing inversion products of vegetation chlorophyll content in key areas around the world

- **Produced 20- meter resolution time-series high-precision vegetation chlorophyll content remote sensing inversion products from 2017 to 2021**

- **The dynamic monitoring product of vegetation chlorophyll content displays the growth status of crops and grassland in key areas at home and abroad.**
- **High-precision, high-resolution chlorophyll inversion products better ensure the quality and competitiveness of the data resources of the special digital earth platform , and are helpful for monitoring crop diseases and insect pests, food yield monitoring , and vegetation growth monitoring.**

Huanghuaihai area

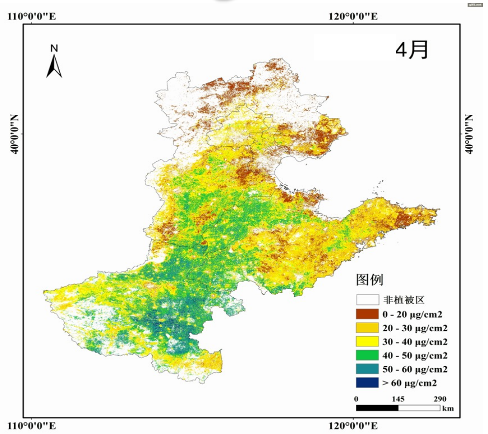

Main grain-producing areas in the middle and lower reaches of the Yangtze River

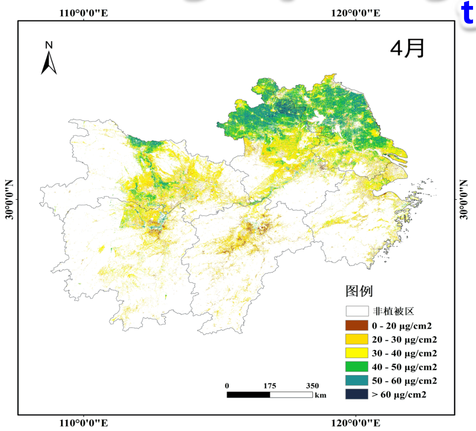

- B. Zhang, H. Ye, Lu. W, et al. Remote Sensing . 2021, 13, 2083. (SCI, Top 25)
- Xiao Yingxin , Dong Yingying, Huang Wenjiang, et al. 2021, UK , 2101354.5. (Patent)

North-east area

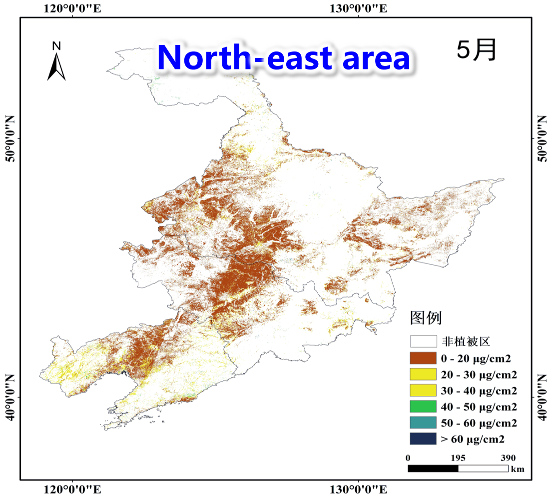

Brazil' s main grain producing areas

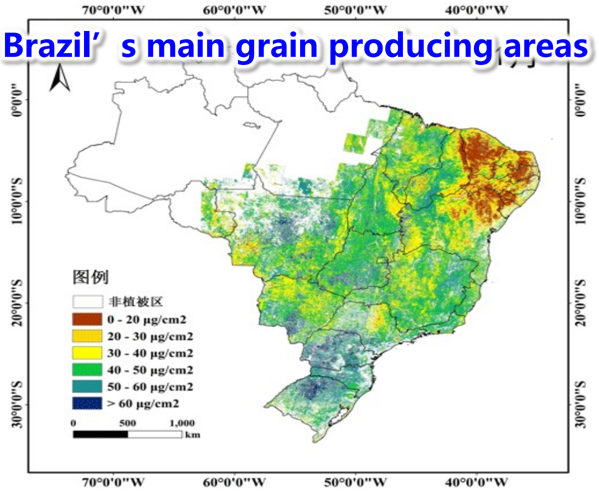

Major food producing areas in the United States

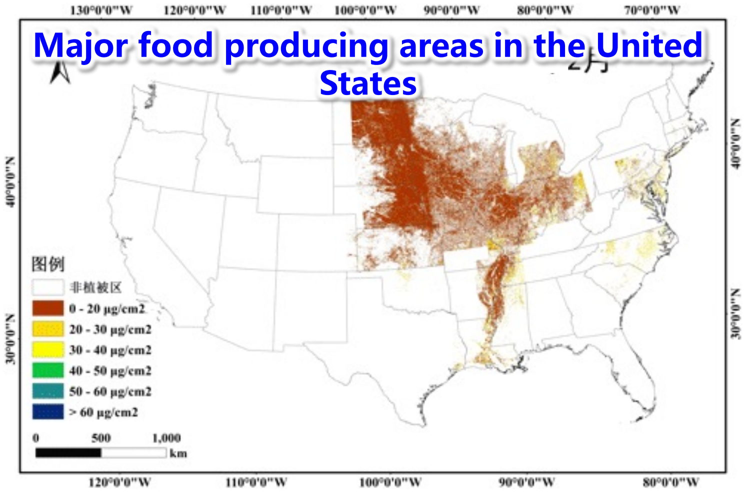

Argentinian grain producing areas

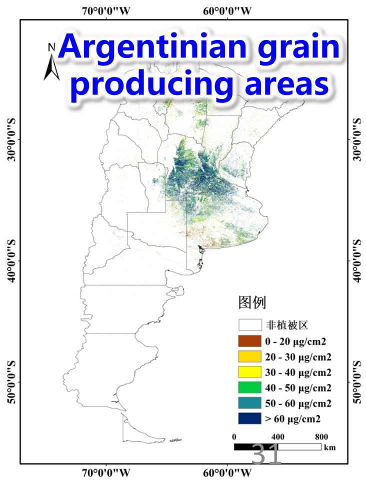

Research Progress

1. Crop monitoring

- Topsoil Characterization
- Crop Biophysical Parameters Retrieval
- Crop Yield Prediction

2. Pest and diseases

- Pest (Locust and Grasshopper Forecasting)
- Diseases (Yellow Rust)

3. Products and Application

Crop Yield Prediction - background

Generating spatial crop yield information is of great significance for academic research and guiding agricultural policy. Existing public yield datasets have a coarse spatial resolution, spanning from 1 km to 43 km, they cannot deal with small-scale spatial heterogeneity, which happens to be the most significant characteristic of the Chinese farmers' economy.

Objectives

To propose a semi-mechanistic model combining remote sensing observations and regional meteorological information, which can simultaneously overcome inter-annual and cross-regional problems.

To generate a high-resolution Chinese winter wheat yield dataset (ChinaWheatYield30m) for the period 2016-2021.

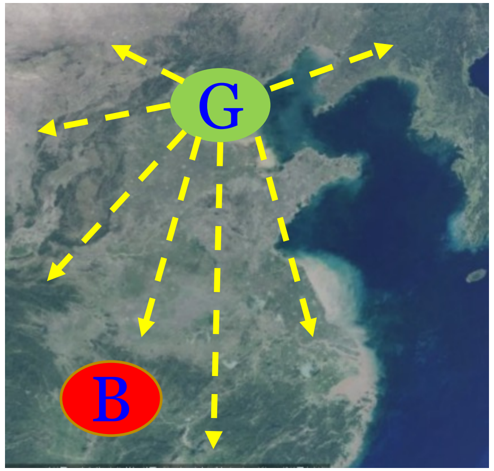

Research content

- Constructing yield model suitable for large area scale
- Analyzing the spatiotemporal scalability of the yield model
- Generating a high-resolution Chinese winter wheat yield dataset

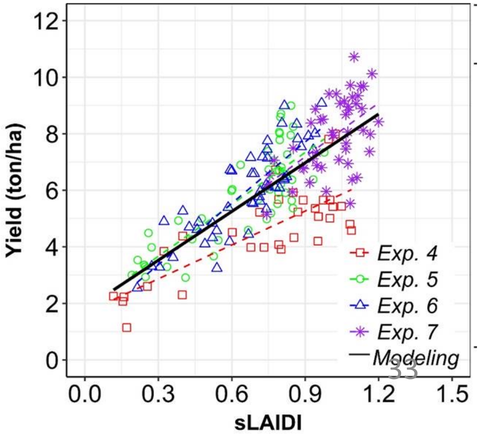

Crop Yield Prediction - Study Area

This study area consists of the main winter wheat-growing region of China.

The main winter wheat production areas are mainly distributed in the Huang-Huai-Hai region (HHH), Southwest China (SW), Gansu-Xinjiang region (GX), the middle and lower reaches of the Yangtze River (MLYR), and the Loess Plateau (LP).

Most of the regions are in the middle of China and includes temperate-continental monsoon, temperate monsoon, and subtropical monsoon climates.

The sown area and production of winter wheat in China accounted for 20.02% of staple food crops in 2021 (National Bureau of Statistics of China, 2021), respectively.

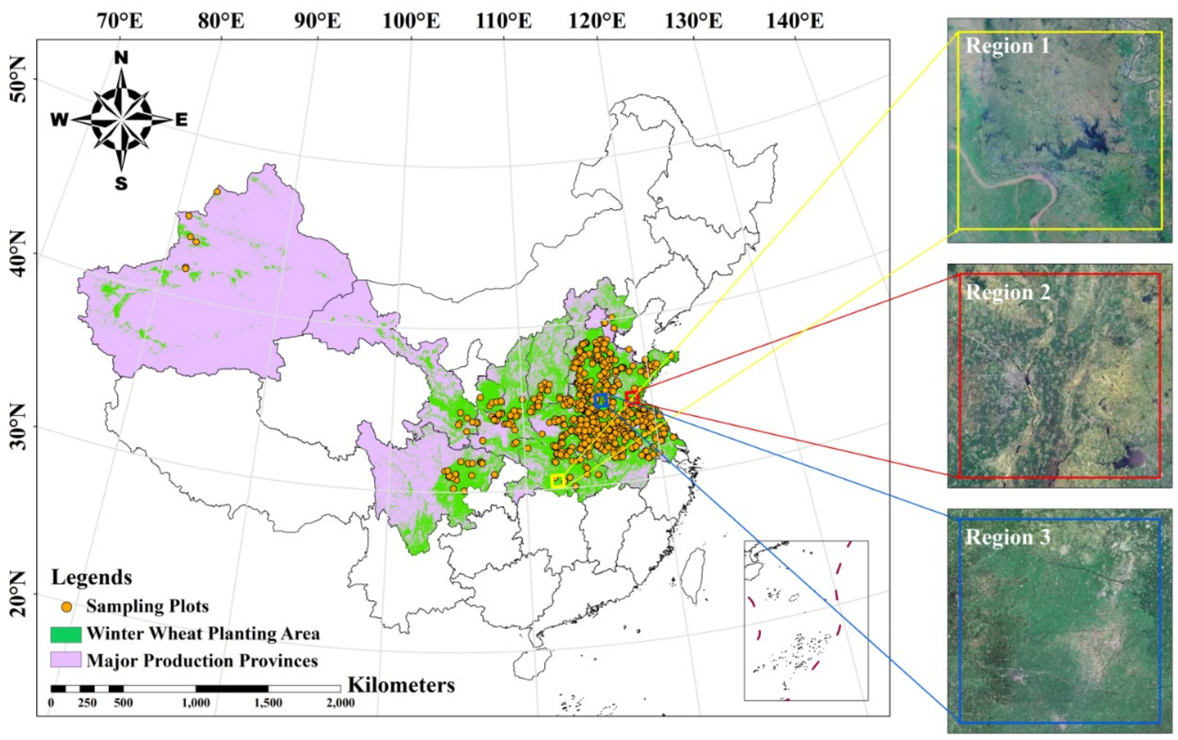

Distribution of winter wheat within the study area and three selected example areas. Region 1, 2, and 3 is available at http://lbs.tianditu.gov.cn/server/MapService.html and represent areas with winter wheat coverages below 25%, around 50%, and above 75%, respectively, serving as representative regions for these respective coverage levels.

Crop Yield Prediction - Result

We generated a 30-m Chinese winter wheat yield dataset (ChinaWheatYield30m) by Hierarchical Linear Modeling (HLM) for major winter wheat region in China for the period 2016-2021.

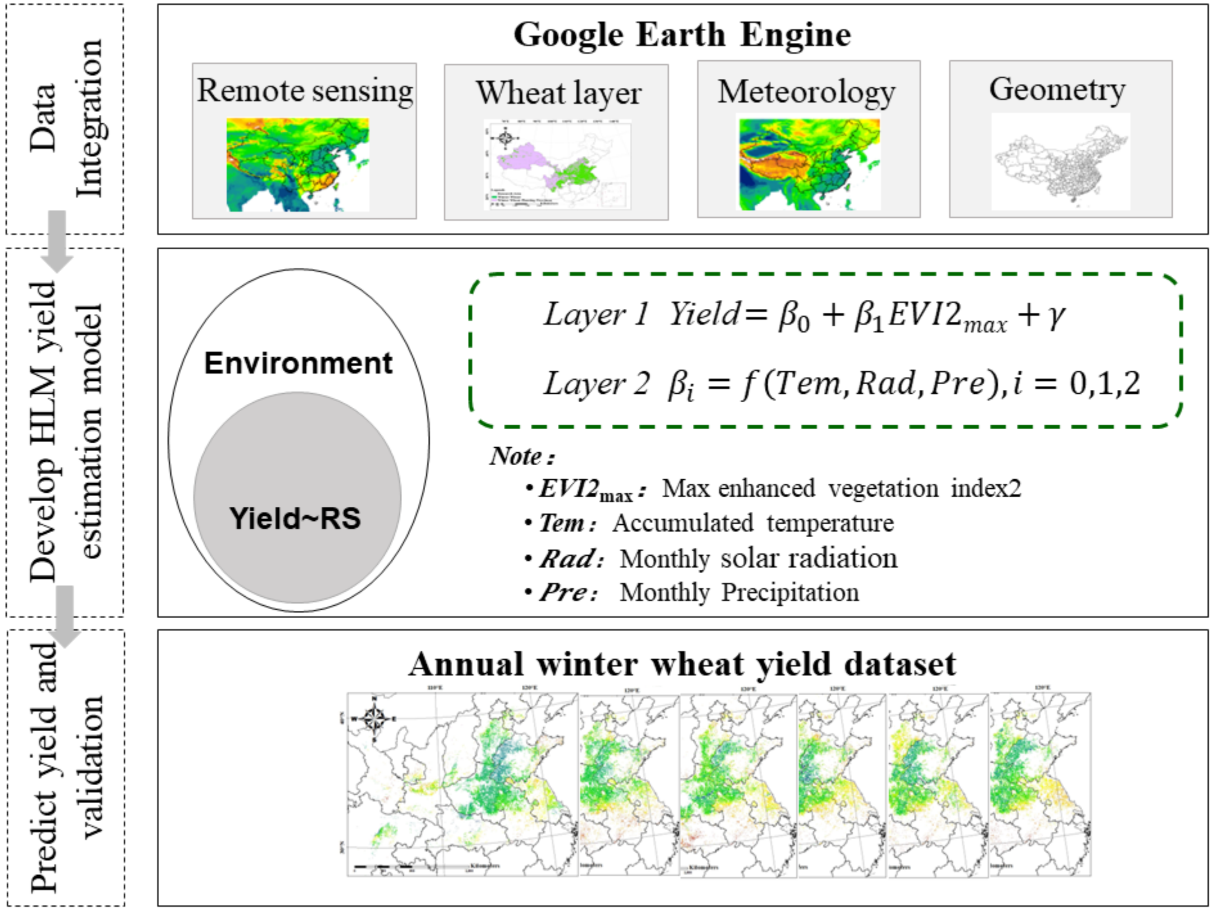

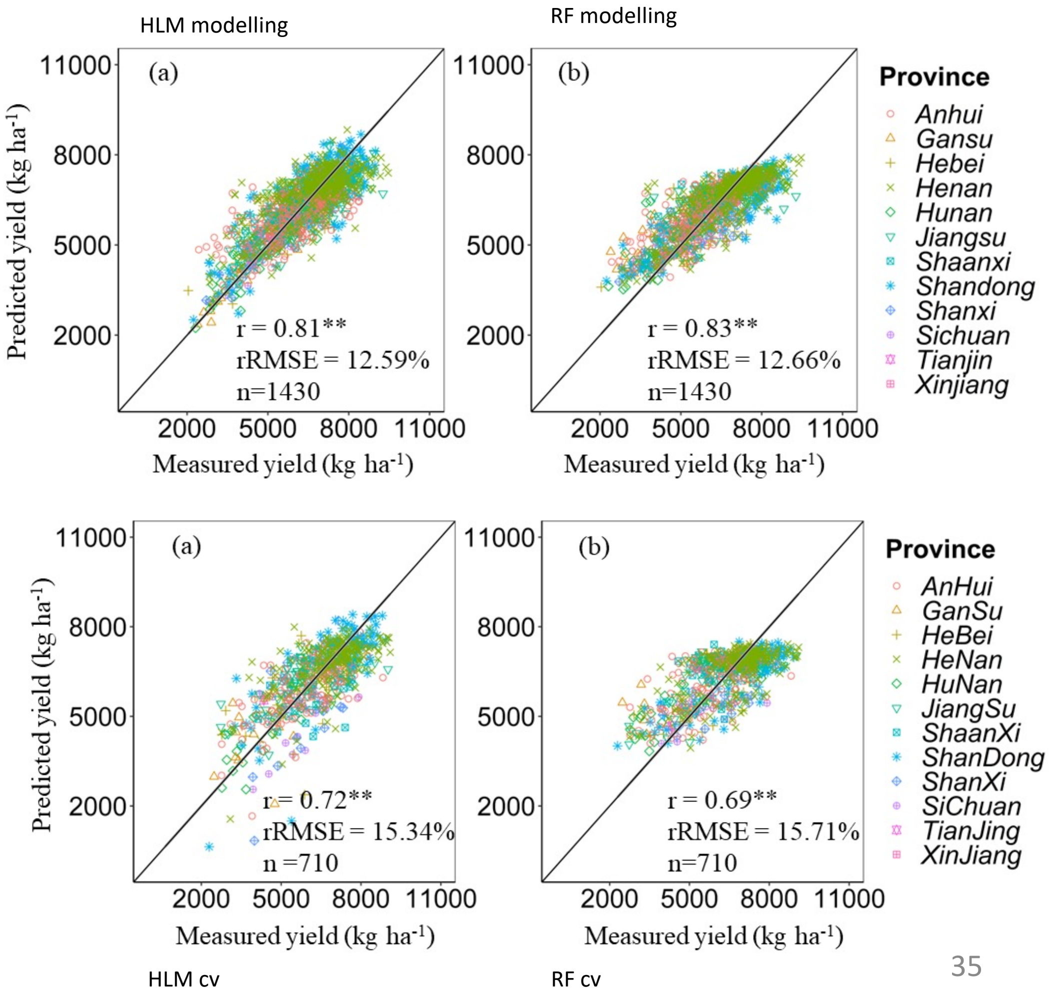

Zenhai-Li et al. RSE 29-022

Crop Yield Prediction - Regional expansion verification

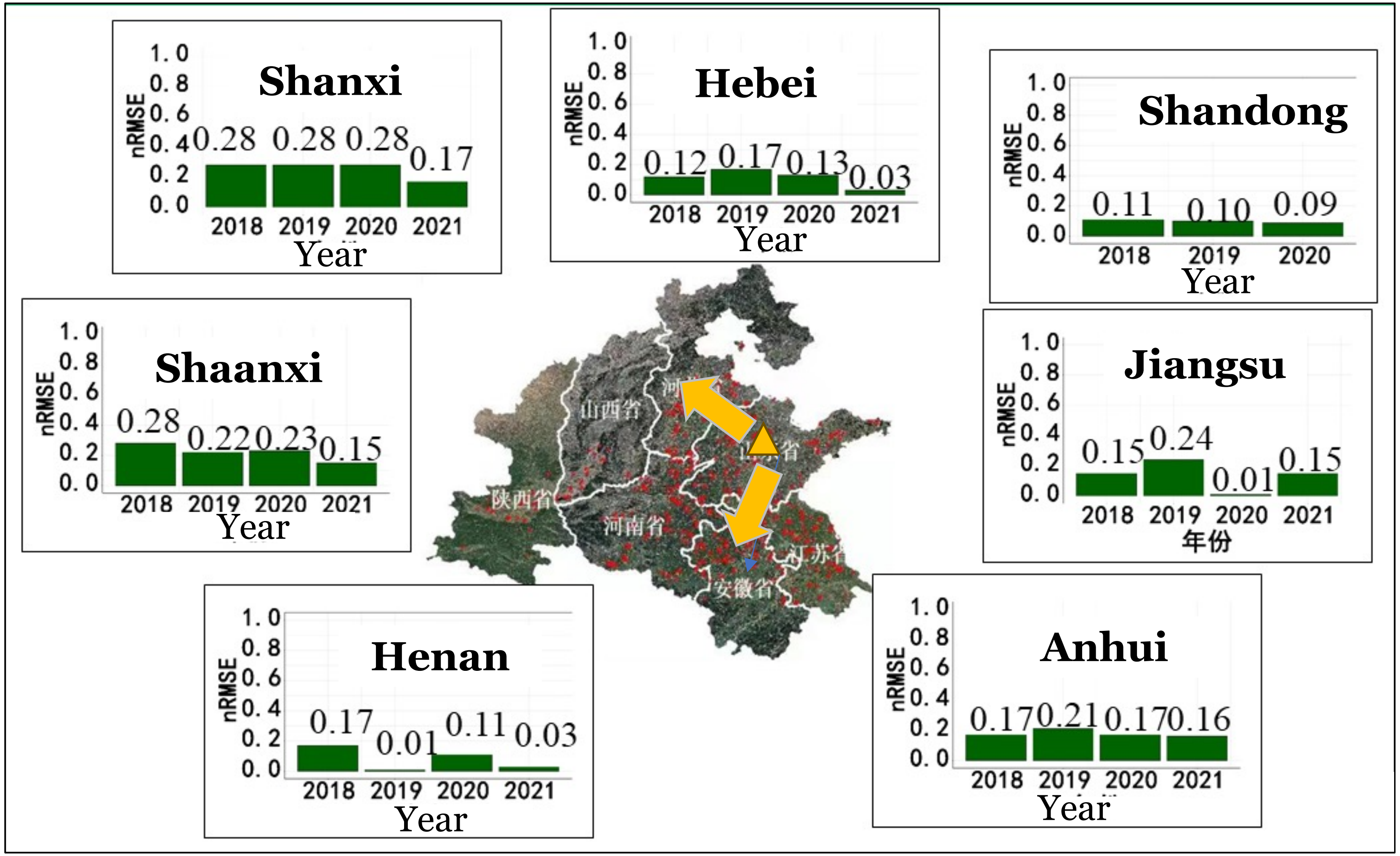

The HLM model demonstrates reliable results in both regional and interannual cross-validation, indicating its good generalizability.

Interannual expansion verification

2018(n=273):0.16

2019(n=225):0.17

2020(n=258):0.17

2021(n=203):0.17

Crop Yield Estimation Based on Remote Sensing Technology

To date, the highest-resolution yield dataset: **ChinaWheatYield30m**

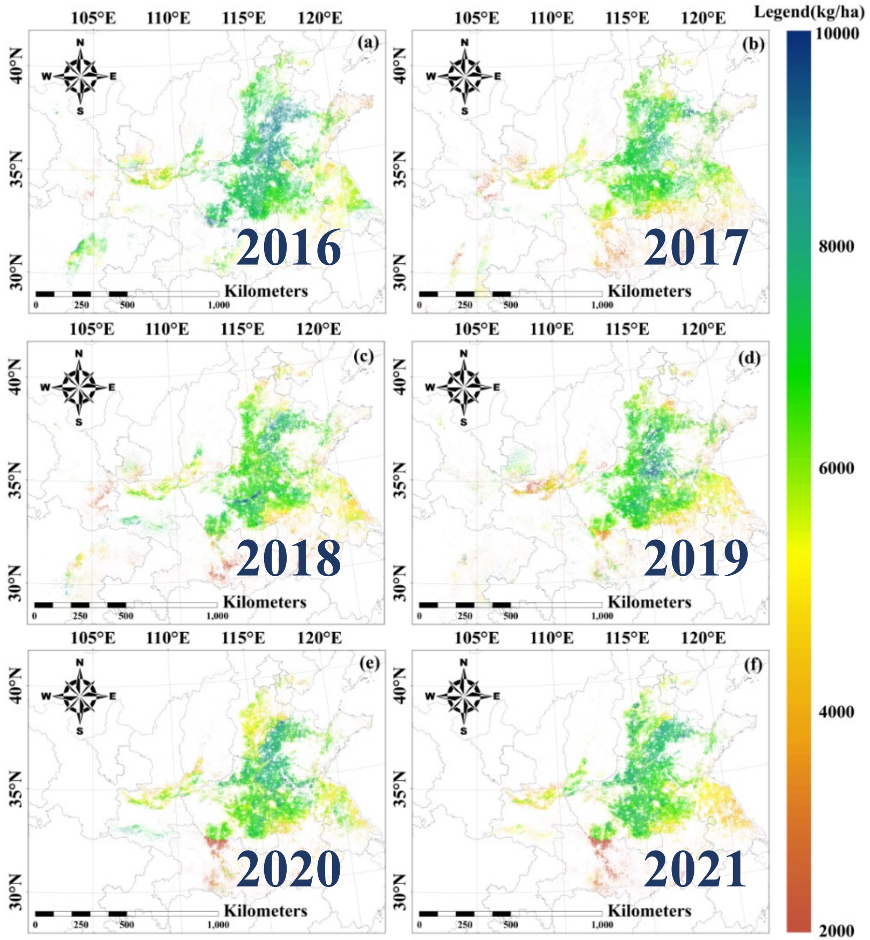

The wheat yield in North China's main province in 2023 has decreased compared to 2022's average yield, consistent with actual production. **—Ministry of agriculture and rural affairs**

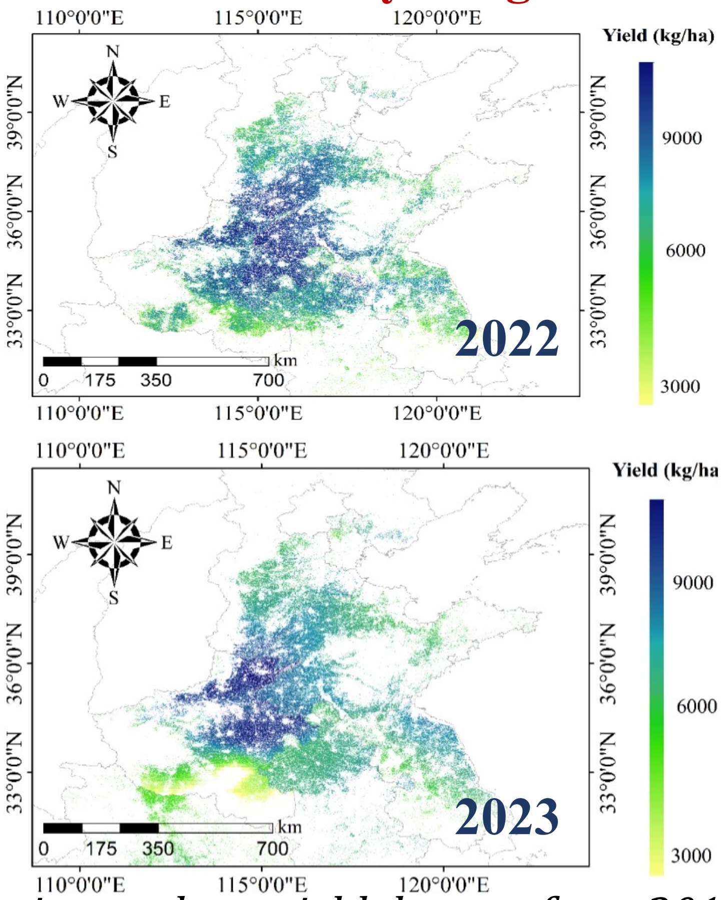

Zhao Y, Han S, Zheng J, et al., ChinaWheatYield30m: A 30-m annual winter wheat yield dataset from 2016 to 2021 in China, Earth system science data, 2023 (Accepted)

Crop Yield Estimation Based on Remote Sensing Technology

First prize

NERCITA

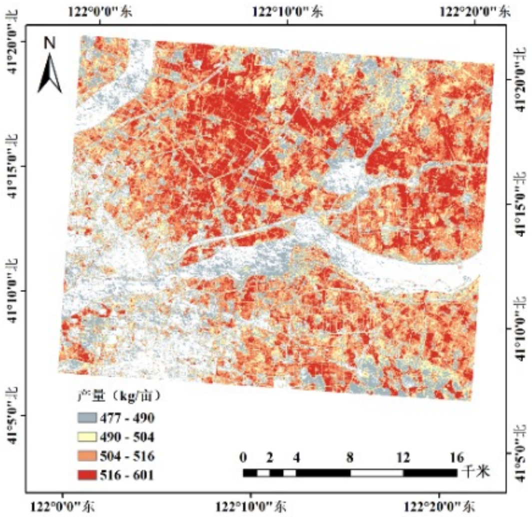

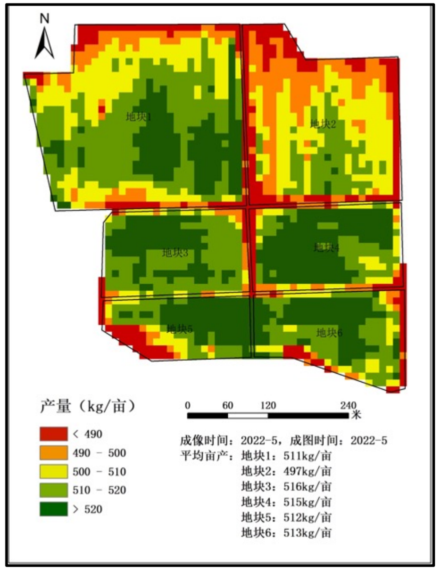

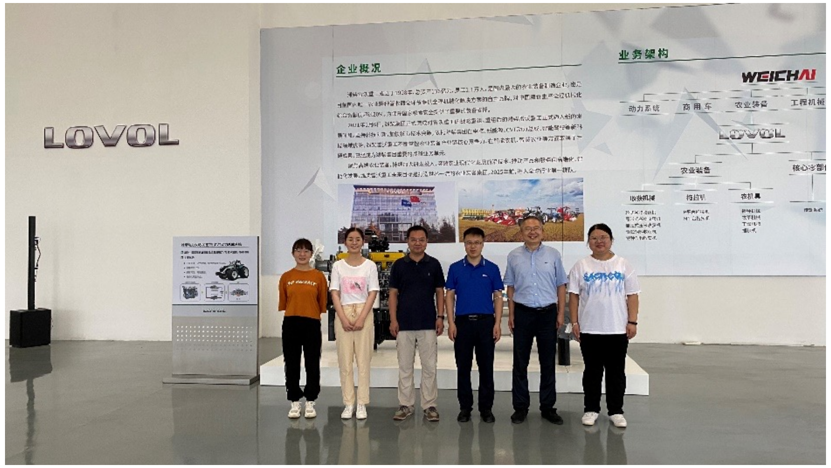

Third-party validation

(by Xianzhengda Company and Weichai Lovol Company) (nRMSE < 15%)

Research Progress

1. Crop monitoring
   - Topsoil Characterization
   - Crop Biophysical Parameters Retrieval
   - Crop Yield Prediction
2. **Pest and Diseases**
   - Pest (Locust Forecasting)
   - Diseases (Yellow Rust)
3. Products and Application

Crop Pest Remote Sensing Monitoring and Forecasting

Locust monitoring and forecasting is of utmost importance due to the devastating impact these insects can have on agriculture and food security. Locust swarms can consume vast quantities of crops, leading to severe food shortages and economic losses.

Forecasting of Locust with global migratory capabilities

Objectives

1 Coupling ground data and remote sensing data to quantitatively analyse the time lag characteristics of key indicators of desert locust occurrence, and to study the extraction methods of indicators.

2 Developing the remote sensing dynamic forecasting model of desert locust occurrence coupled with multiple indicator factors to achieve early warning of desert locus.

Research content

- Extraction of multivariate indicators required for early warning of desert locust occurrence
- Analysis of the lagged response of desert locust occurrence to indicators
- Early warning of the risk of desert locust occurrence

Desert Locust Forecasting - Study Area

This study concerns Somalia, Ethiopia, and Kenya (SEK) in the Great Horn of Africa. It extends eastwards to the Arabian Sea, across the Gulf of Aden from Yemen.

SEK can form complementary breeding areas activated by either spring, summer, or winter rains. Since 2018, the Indian Ocean Dipole.

They brought SEK extraordinary rainfall (2018-2019), providing suitable conditions for desert locust breeding. Mass migration of swarms from the Arabian Peninsula since June 2019 has culminated in an outbreak of desert locusts in SEK.

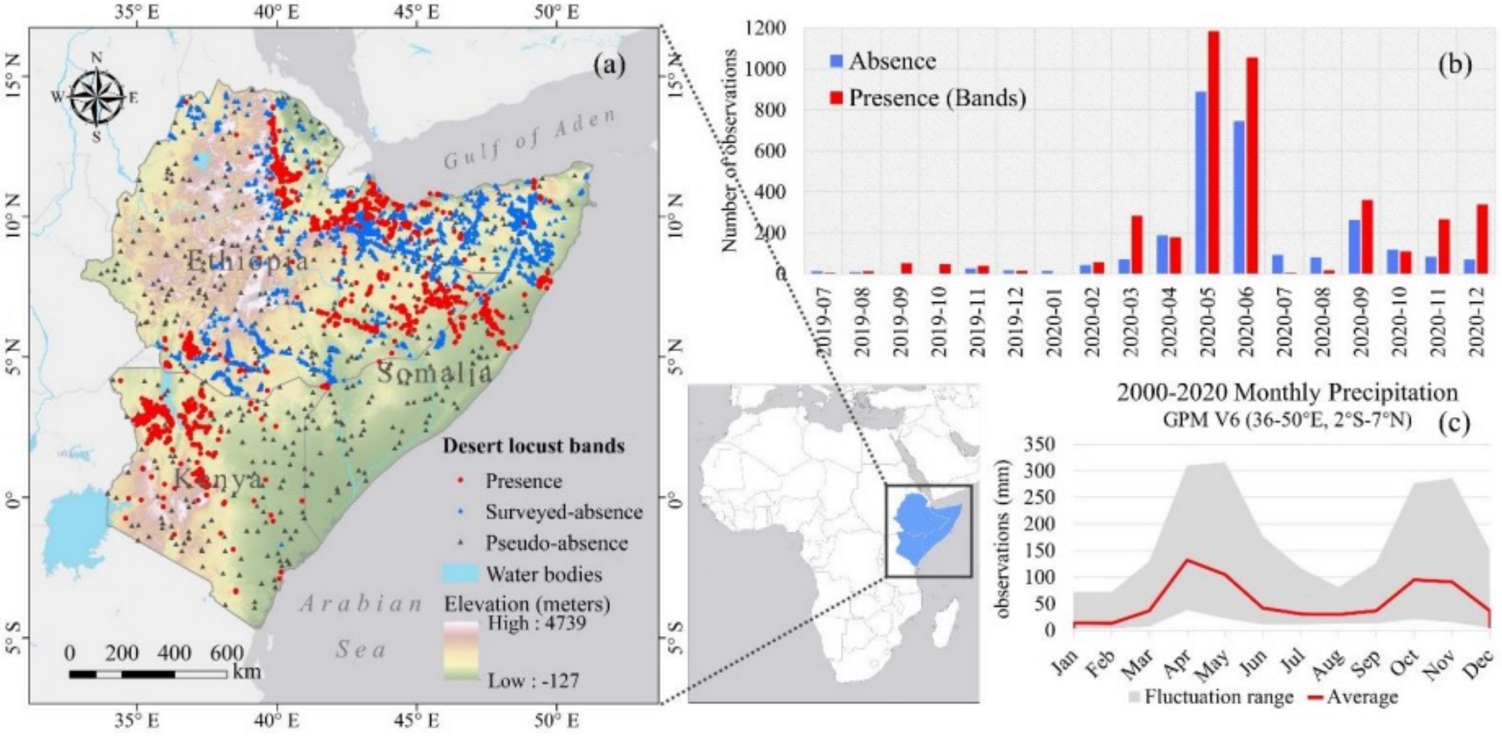

Spatial and temporal distribution of ground points of the desert locust band used for this study in the SEK region. (a) The geographical location of SEK with band observations in 2000-2020; the red dot represents band presence while the blue triangle refer to surveyed-absence and the grey one indicates pseudo-absence. (b) Monthly count of bands from July 2019 to December 2020. (c) Monthly observations of Global Precipitation Measurement(GPM) V6 in the central SEK region for 20 years(2000-2020); the red line indicates monthly mean rainfall; the grey area indicates the fluctuation interval.

Analysis of time lagged effects of indicator factors

Rainfall

The surge in rainfall observed 41-64 days before the onset of the desert locust is a signal for females to lay eggs and can also promote vegetation growth, which ultimately affects locust corm growth and development

Soil moisture

The increase in soil moisture from 73-80 days before occurrence to 33-40 days before occurrence is a booster of locust egg hatching and an early signal of vegetation growth

NDVI

The increase in NDVI during the 17-40 days prior to locust infestation acts as a food source and habitat for locust cysts during their developmental phase, influencing their growth, development and distribution and aggregation, as well as an ecological response to meteorological conditions such as precipitation

LST

The 89-96 days and 17-24 days of LST prior to locust infestation influenced egg hatching rates, mortality and development rates, and therefore acted on both the pre- and post-desert locust development process

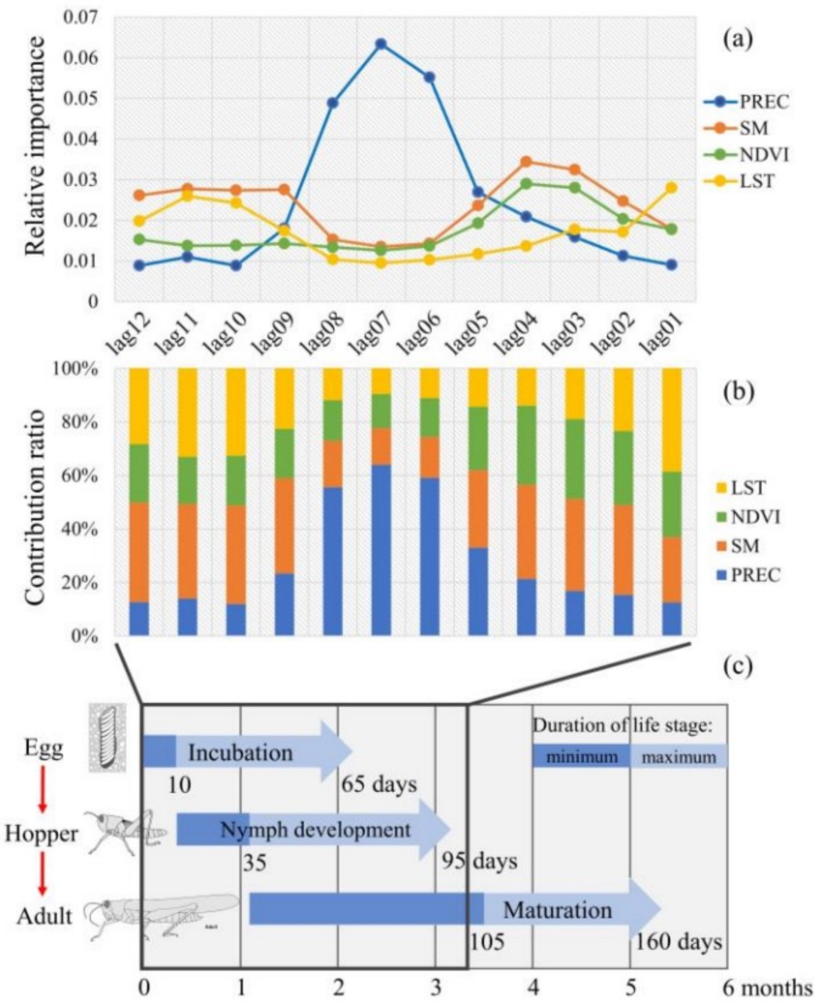

Model for Forecasting Based on a Temporal Sliding Window

SVM was used as the fundamental model for the forecast for a better overall accuracy throughout the years.

For dynamic indicators, a temporal sliding window selector was selected to choose trainers and predictors dynamically based on the time lag information mining from the historical ground survey information and long time series of satellite.

Lagging variables of dynamic indicators with lower significance were removed and those that contributed highly survived. We then combined other static indicators for model training and prediction.

A data-driven multivariate approach was proposed combining machine learning and a temporal sliding window to predict band occurrence for early.

Multivariate forecasting model training

SVM

↓

Dynamic forecasting of band occurrence

SVM+temporal sliding window of dynamic predictors

↓

Accuracy evaluation and discussion

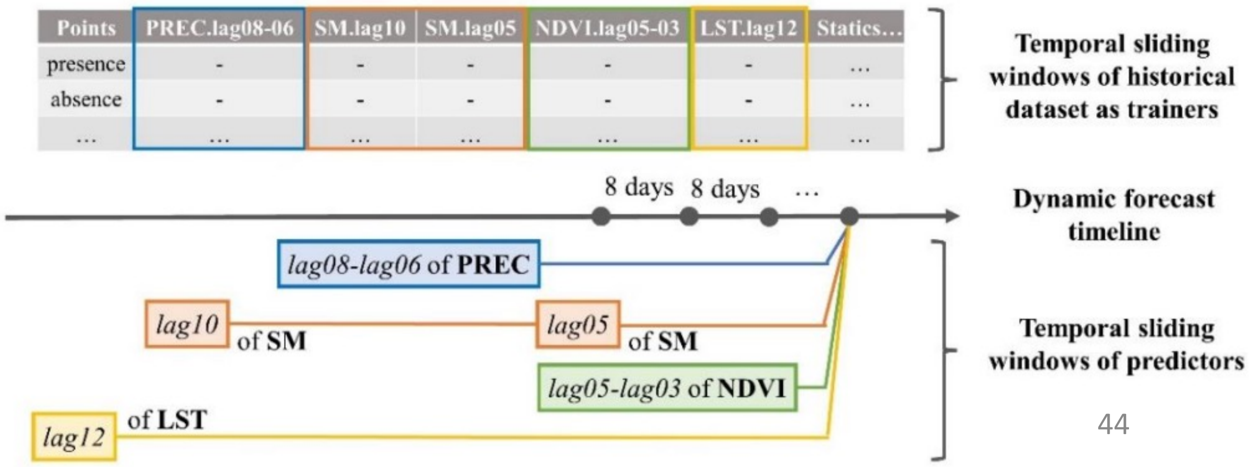

Model Evaluation and Accuracy Assessment

Dynamic optimal segmentation → Confusion matrix construction → Calculation of precision indicators

- **Dynamic optimal segmentation:** the probability threshold corresponding to the Kolmogorov-Smirnov (KS) statistic (max TPR+TNR) of the training model is used as the optimal segmentation point to map the prediction results to binary classification results (with/without risk)
- **Confusion matrix construction:** the occurrence points of each month reserved from the training set are superimposed on the classification results as ground truths, and the occurrence points falling into the risk zone are recorded as true positives; the absence points falling into the non-risk zone are recorded as true negatives
- **Calculation of precision indicators:** accuracy, sensitivity, specificity, ROC-AUC, precision and F1 score were selected as indicators

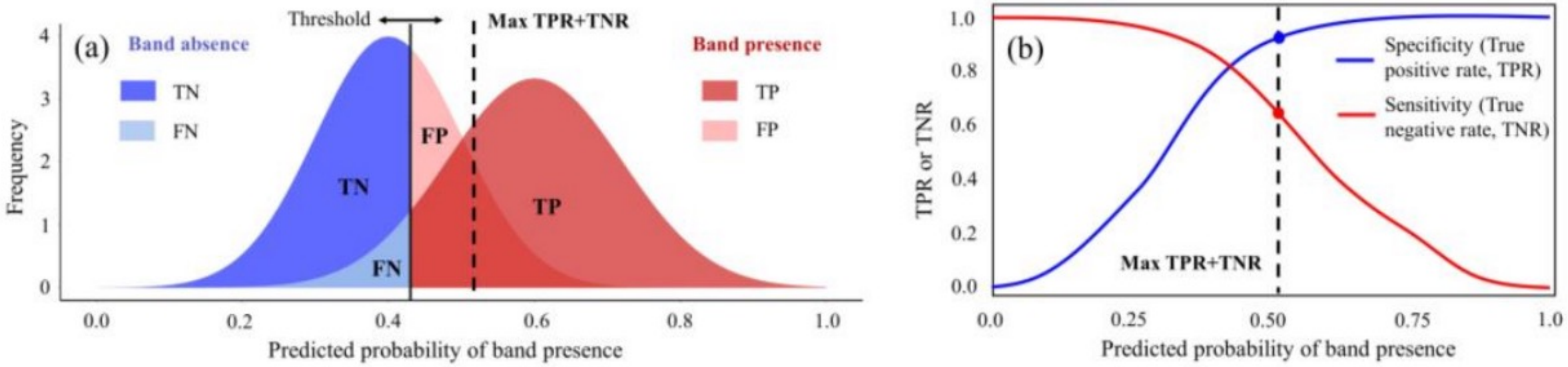

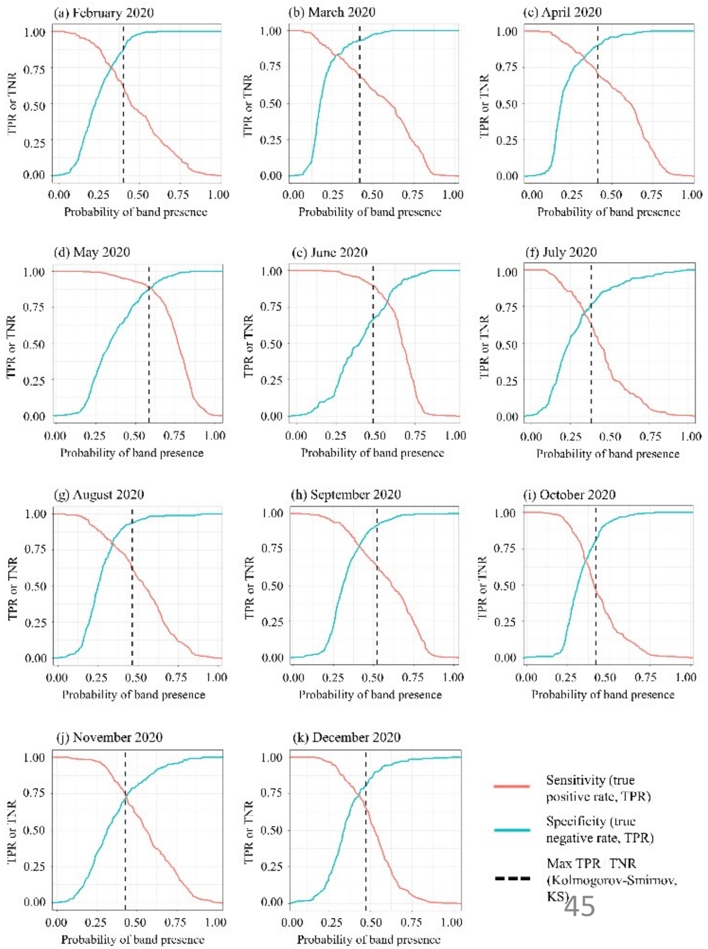

Dynamic Forecasting of Desert Locust

Eleven forecast experiments from February to December 2020 demonstrated satisfactory overall performance with an average accuracy of **77.46%,** a ROC-AUC value of **0.7666**, and an F-score close to **0.7715**. The forecast accuracies for March, April, May, and June were exceptionally high, above 80%.

Date	Evaluation Metrics				
	Accuracy (%)	Sensitivity	Specificity	ROC-AUC	F-Score
February 2020	74.44	0.6047	0.8759	0.7403	0.7792
March 2020	80.15	0.6934	0.9329	0.8131	0.7930
April 2020	82.59	0.7264	0.9002	0.8133	0.7811
May 2020	88.68	0.8886	0.8814	0.8850	0.9218
June 2020	85.31	0.8971	0.6667	0.7819	0.9081
July 2020	70.00	0.6167	0.7714	0.6940	0.6549
August 2020	76.99	0.6238	0.9412	0.7825	0.7453
September 2020	79.81	0.6314	0.9203	0.7759	0.7258
October 2020	66.77	0.5988	0.7419	0.6704	0.6515
November 2020	73.41	0.7500	0.7116	0.7308	0.7673
December 2020	73.95	0.7087	0.7816	0.7451	0.7586
Average	77.46	0.7036	0.8296	0.7666	0.7715

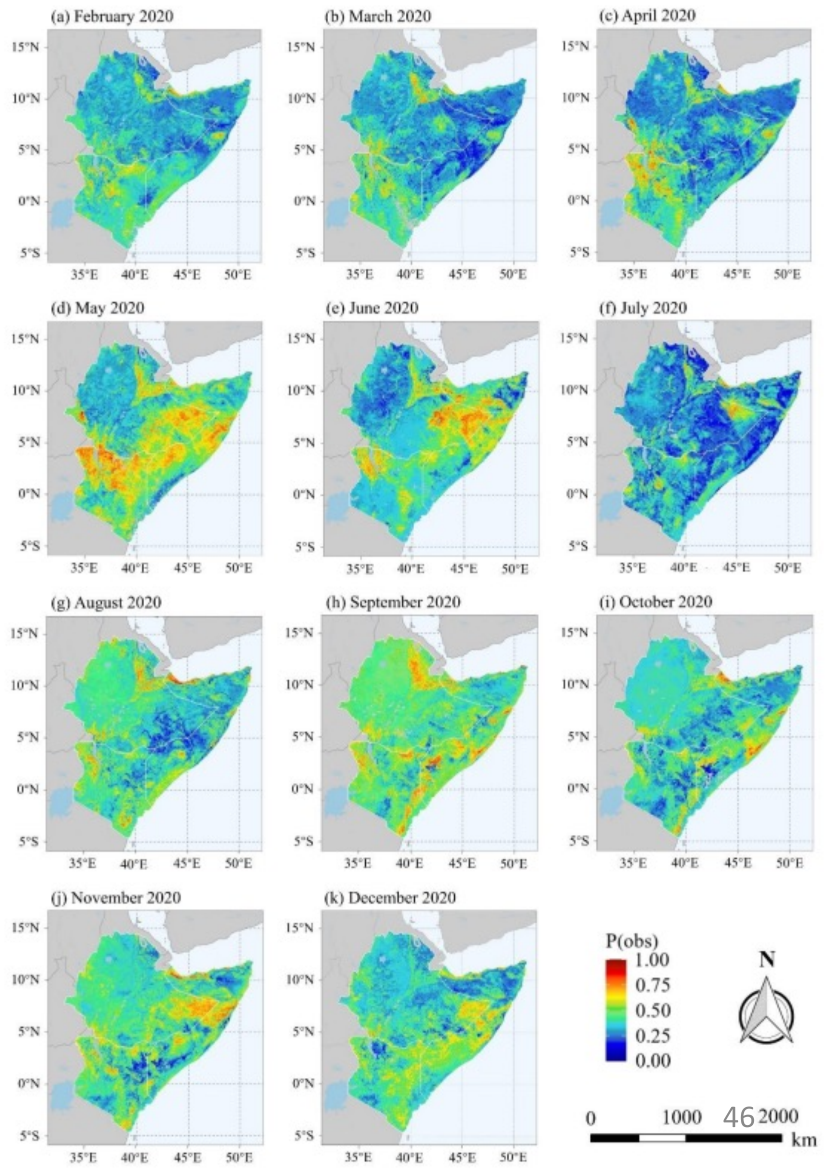

Research Progress

1. Crop monitoring
   - Topsoil Characterization
   - Crop Biophysical Parameters Retrieval
   - Crop Yield Prediction

2. **Pest and Diseases**
   - Pest (Grasshopper Forecasting)
   - Diseases (Yellow Rust)

3. Products and Application

Monitoring for Locust migrating in small areas

Objectives

1. Detect the environmental factors, including meteorological, vegetation, topographic, and soil factors, that affect the developmental stages of grasshoppers ;
2. Extract the grasshopper potential suitable habitat associated with meadow and typical steppes;
3. Analysis spatial-temporal characteristics of the grasshopper potential suitable habitat
4. Explored the effects of the habitat factors in two steppe types.

Research content

- extract the distribution of the grasshopper potential habitat
- analyze the spatial-temporal characteristics of the grasshopper potential habitat
- detect the different effects of key environmental factors in the meadow and typical steppe

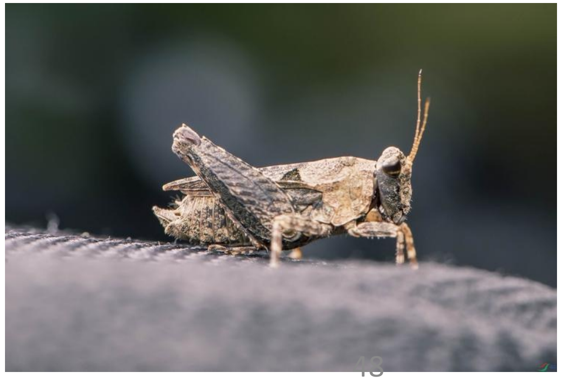

Study Area

In this study, **two major steppe types** of Xilingol league (42°32′~46°41′N, 111°59′~120°00′E) were selected as the study area (Figure a):

- **meadow steppe** (Figure b)
- **typical steppe** (Figure c).

The meadow steppe in the Xilingol often occurs on Castanozem and saline-alkalized soils with poor fertility. The dominant grass *L. chinensis* has strong colonization capability.

In the typical steppe, the most abundant grasses were *Stipa Grandis* and *Achnatherum sibiricum*, which are more favored by grasshoppers. Additionally, compared with the meadow steppe, the fractional vegetation coverage is lower in the typical steppe. Therefore, it is **easier to cause grasshopper infestation**.

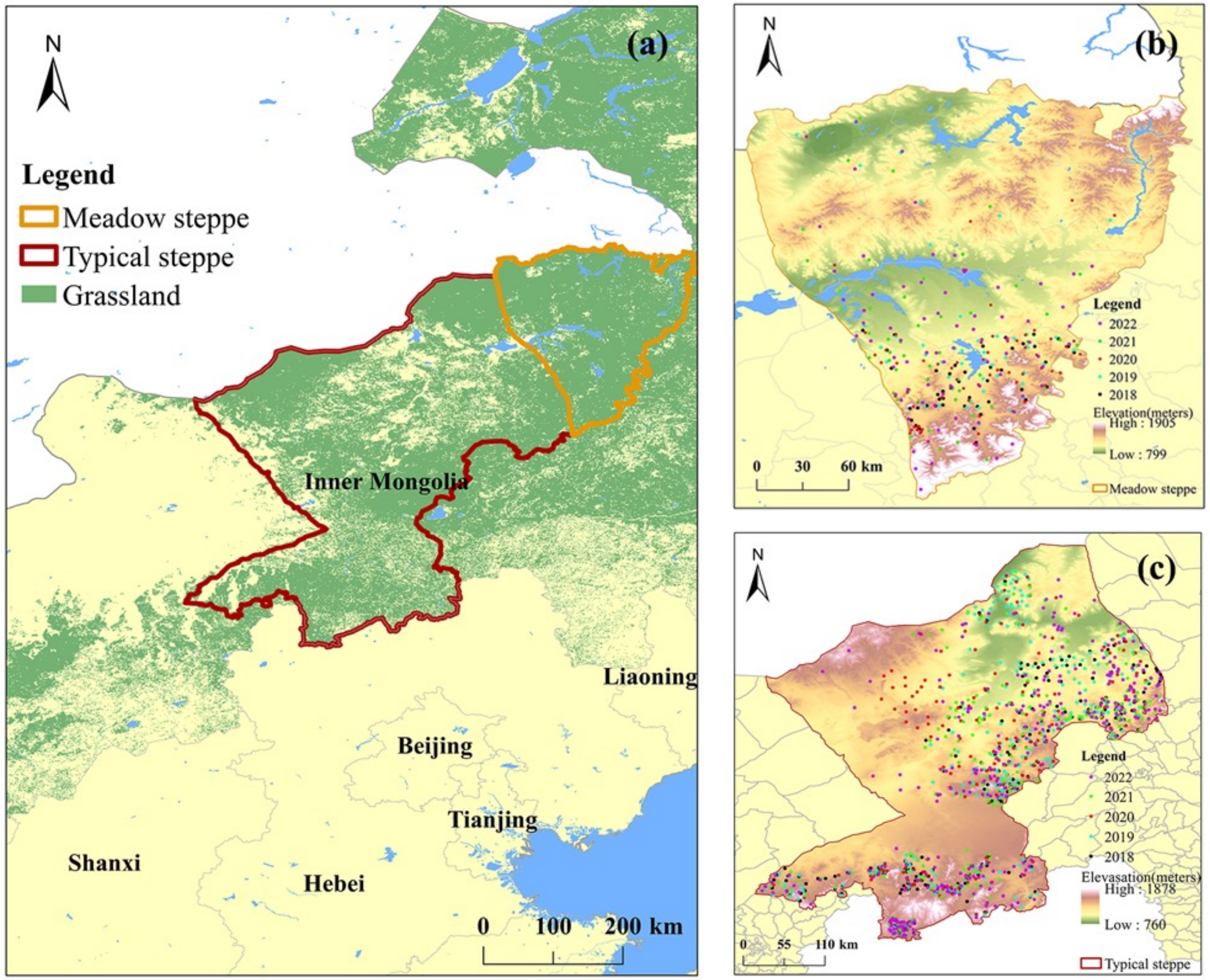

(a) Location of the study area; (b) location of the meadow steppe area and grasshopper occurrence points from 2018 to 2022; and (c) location of the typical steppe area and grasshopper occurrence points from 2018 to 2022.

Grasshopper Forecasting - Select Influence factors

The growth and occurrence of grasshoppers are affected by the climate, soil, vegetation, and topography. Through the correlation between factors, **14** habitat factors were selected to extract the grasshopper potential suitable habitat.

Environmental variables influencing grasshoppers in each developmental stage.

Category	Environmental Variables	Detailed Description of Environmental Variables	Spatial Resolution
Topography	Elevation		90 m
	Slope		90 m
	Aspect		90 m
Meteorology	Land surface temperature	Minimum land surface temperature in the egg stage (EMinLST); nymph stage (NMinLST) Mean land surface temperature in the nymph stage(NMeanLST); adult stage(AMeanLST)	1 km
	Precipitation	Precipitation in the egg stage (EPre) Precipitation in the nymph stage (NPre) Precipitation in the adult stage (APre)	0.1°
	Soil temperature	Soil temperature in the egg stage (EST) Soil temperature in the nymph stage (NST) Soil temperature in the adult stage (AST)	1 km
Vegetation	Vegetation type		1 km
	Aboveground biomass	Aboveground biomass in the nymph stage (NAB) Aboveground biomass in the adult stage (AAB)	1 km
Soil	Soil type		1 km
	Soil salinity index	Soil salinity in the egg stage (ESI) Soil salinity in the nymph stage (NSI) Soil salinity in the adult stage (ASI)	1 km

Correlation calculate

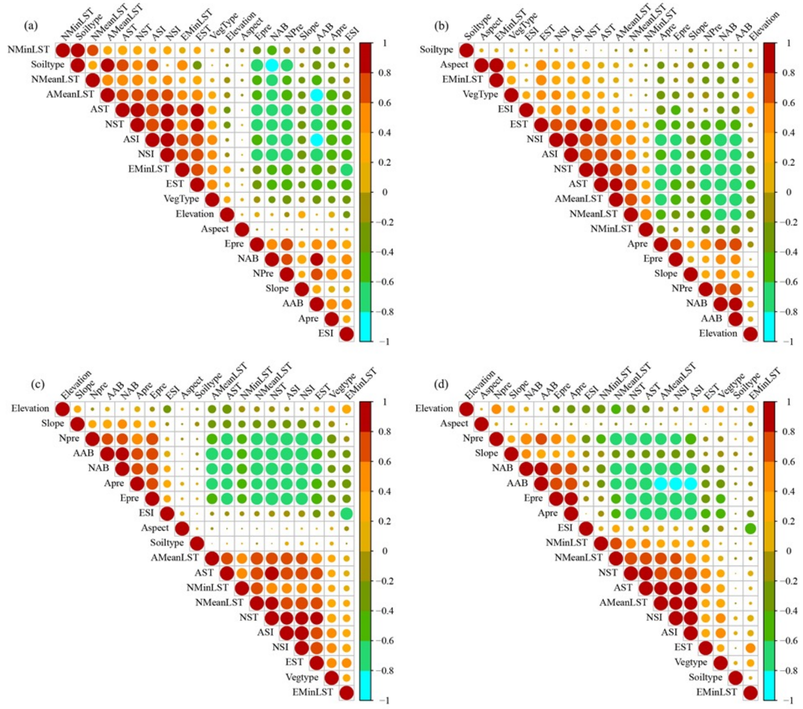

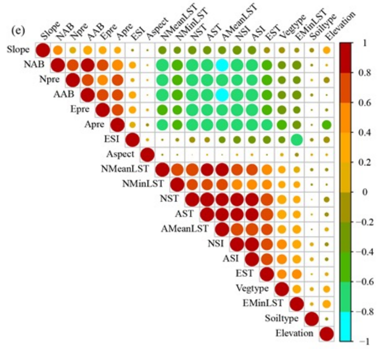

Environmental factor correlation results from 2018 to 2022.
(a) 2018;
(b) 2019;
(c) 2020;
(d) 2021;
(e) 2022

Grasshopper Forecasting

Extraction Method of Grasshopper Potential Suitable Habitat

- MaxEnt was applied to extract the distribution of grasshopper potential suitable habitat.
- Grasshopper potential suitable habitat maps were generated using the **bootstrap approach** with replicates set to **50**;
- Training (70%) and testing (30%) datasets has been set for each year;
- Model accuracy was evaluated in terms of the omission rate and predicted area (ORPA) and the area under the curve (AUC) of the receiver operating characteristic (ROC) curve;
- Three levels of possibility were set: less suitable (0–0.5), moderately suitable (0.5–0.7), and most suitable (0.7–1).

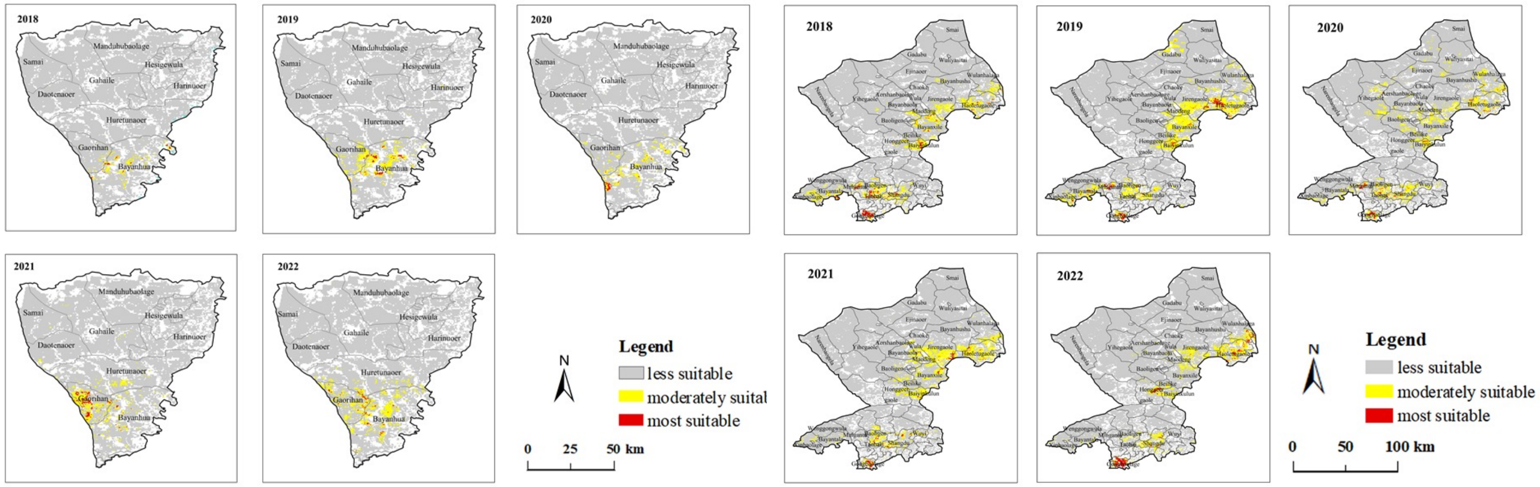

Spatial distribution of the GPHs in the meadow and typical steppe from 2018 to 2022

Year	Area of Meadow Steppe (km²)			Area of typical Steppe (km²)		
	Most Suitable	Moderately Suitable	Less Suitable	Most Suitable	Moderately Suitable	Less Suitable
2018	44	407	32,853	1091	8829	110,098
2019	101	1135	32,068	1055	12,460	106,503
2020	64	691	32,549	686	10,341	108,991
2021	192	1218	31,894	672	10,854	7491
2022	102	1622	31,580	1192	7491	111,335

Areas of each suitability level in the meadow and typical steppes from 2018 to 2022.

Temporal Variation Characteristics of Grasshopper Potential Suitable Habitat

- the suitability index changes corresponding to each pixel were analyzed;
- the significance of these changes was tested according to the F value from 2018 to 2022.
- Only the trends that passed the F test had significant p values, meaning that the trend of the suitability index changed. The p value selected for this study was 0.1, meaning that at this level, the trend at least marginally significantly changed.

Main Influencing Factors in the Meadow and Typical Steppes

- We regarded the factors with cumulative contributions exceeding 80% as the main influence factors.
- EST, soil type, vegetation type are the same important factors for two steppes ;

In the meadow steppe, the EST, vegetation type, soil type, and aspect were the vital factors

In the typical steppe, the vegetation type, EST, soil type, and NPre were the vital factors

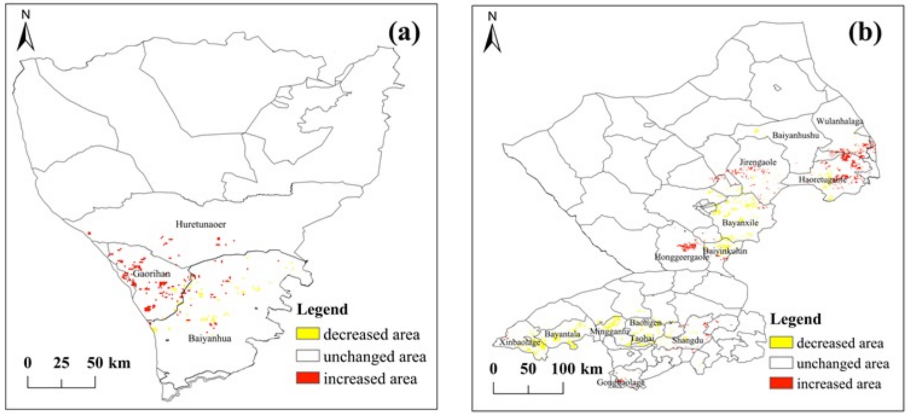

(**a**) The trends of the suitability index in meadow grasslands; and (**b**) typical steppe.

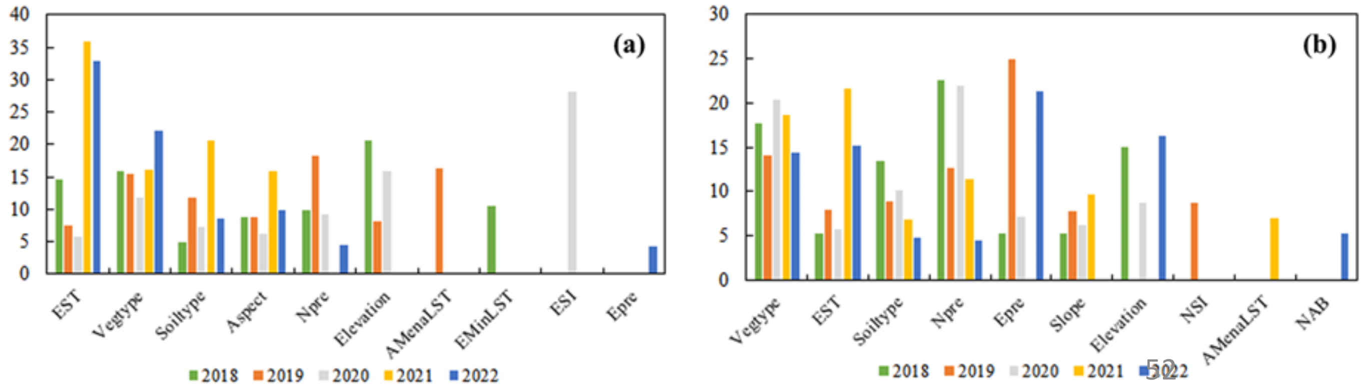

environmental factors contributions from 2018 to 2022 in the (**a**) meadow steppe, and (**b**) typical steppe.

Research Progress

1. Crop monitoring
   - Topsoil Characterization
   - Crop Biophysical Parameters Retrieval
   - Crop Yield Prediction

2. **Pest and Diseases**
   - Pest (Locust and Grasshopper Forecasting)
   - Diseases (Yellow Rust)

3. Products and Application

Field data collection campaigns – Crop Disease

Data on crop (wheat and maize) areas affected by yellow rust have been collected by exploiting the opportunity offered by the participation to another ESA funded project (**Afri4Cast**).

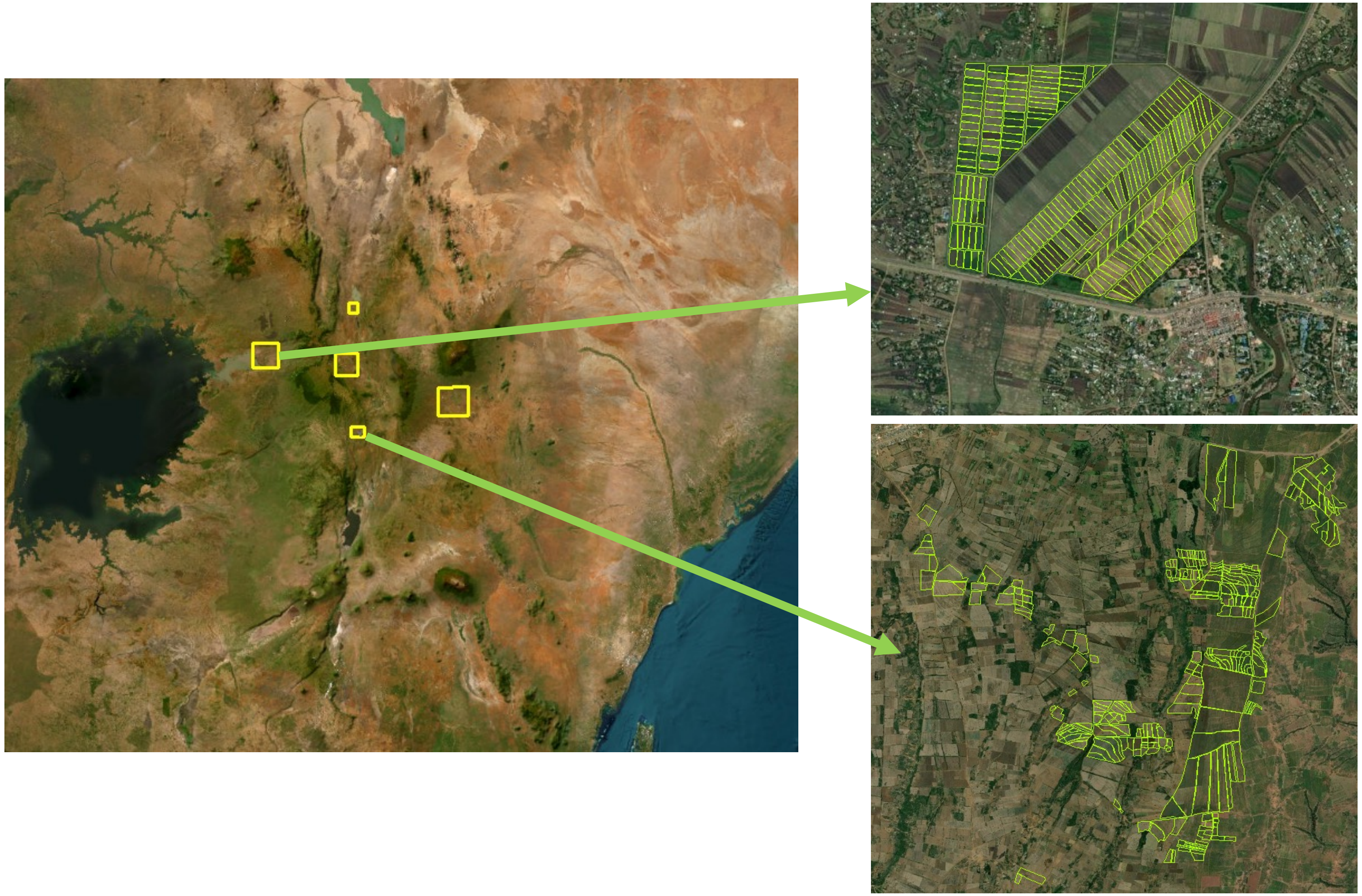

Up to now two field campaigns have been carried out in collaboration with the University of Nairobi:

5 – 17 June 2023 & 9 – 18 July 2023

Parameter	Crop	Target	Completed
Parcel mapping	Maize	200	151
	Wheat	0	128
	Rice	200	252
Rust scoring	Maize	100	51
	Wheat	0	52
	Rice	0	0
LAI	Maize	50	51
	Wheat	50	52
	Rice	50	74
Chlorophyll	Maize	0	51
	Wheat	0	52
	Rice	0	74

Yellow rust detection and monitoring

For what concerns crop threats, the core of the system aiming at detecting yellow rust outbreaks in maize and wheat crops, will be built on S2 and PRISMA satellite.

Several VIs (NDVI, SIPI, PRI, PSRI, MSR) computed by using multispectral and hyperspectral images has been used to implement a Diseases Infection Index (DII).

Objectives

Coupling ground data and remote sensing data to quantitatively the presence of yellow rust in wheat and maize agricultural fields.

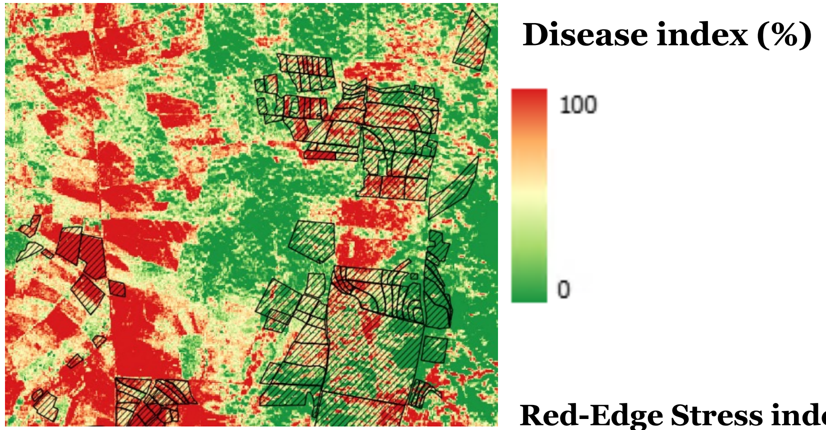

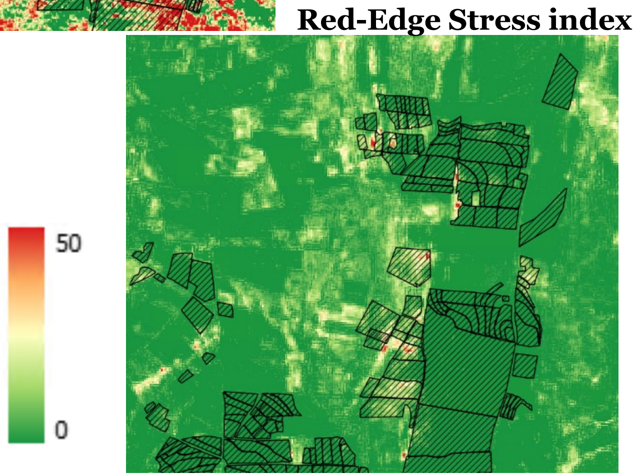

Research content

- ➢ Extraction of multivariate indicators required for early detection of yellow rust.
- ➢ Validation of the indicators through field data.
- ➢ Crop type maps and maps of yellow rust potential presence on wheat and maize

Yellow rust detection and monitoring

Narok county, Kenya – 12/06/2023

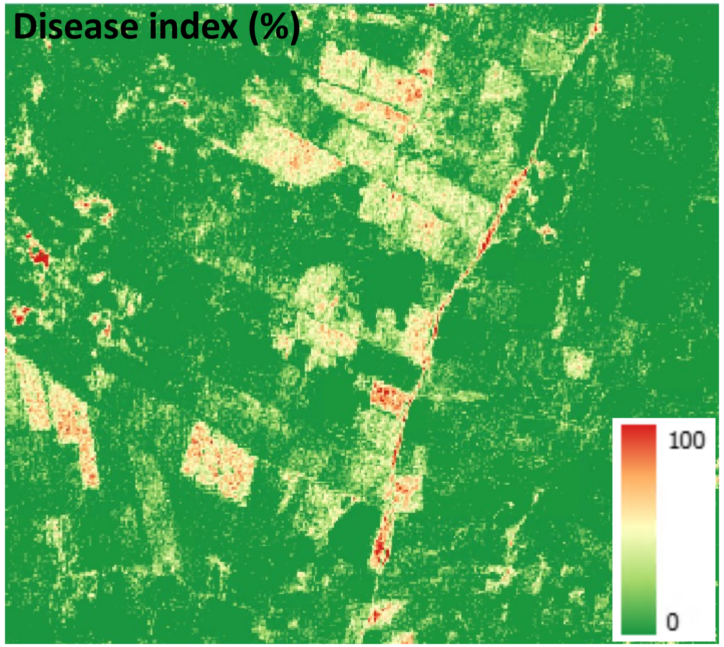

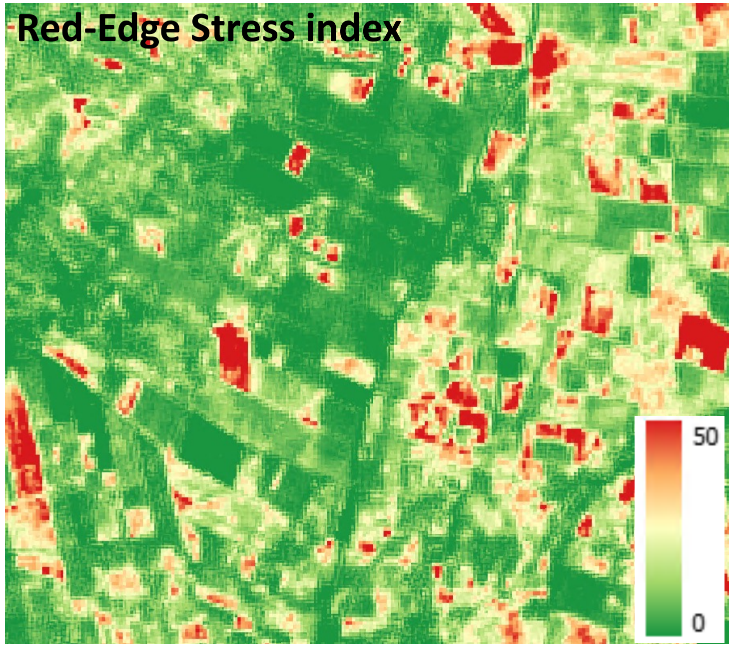

Disease infection index (mid-season because taken in the months of full growth of wheat and maize in Kenya) and the red edge stress index are shown.

Scales range from to 100 % for DII like probability of infection.

While for the red edge, higher than 50-60 there should be a correlation with the rust.

Results have not been validated yet.

Research Progress

1. Crop monitoring
   - Topsoil Characterization
   - Crop Biophysical Parameters Retrieval
   - Crop Yield Prediction

2. Pest and Diseases
   - Pest (Locust and Grasshopper Forecasting)
   - Diseases (Yellow Rust)

3. Products and Application

Products and Application

Based on the above achievements, we have successfully monitored the major **breeding areas and migration paths** of desert locust in the Asia-Africa region from 2018 to 2023. We have also conducted remote sensing monitoring of disaster situations in key affected countries and continuously updated the dynamics of their impact. This has provided vital information support for locust disaster emergency response. Our analysis has revealed that **Pakistan, Yemen, and countries in the Horn of Africa such as Somalia, Ethiopia, and Kenya** are among the most severely affected by desert locust.

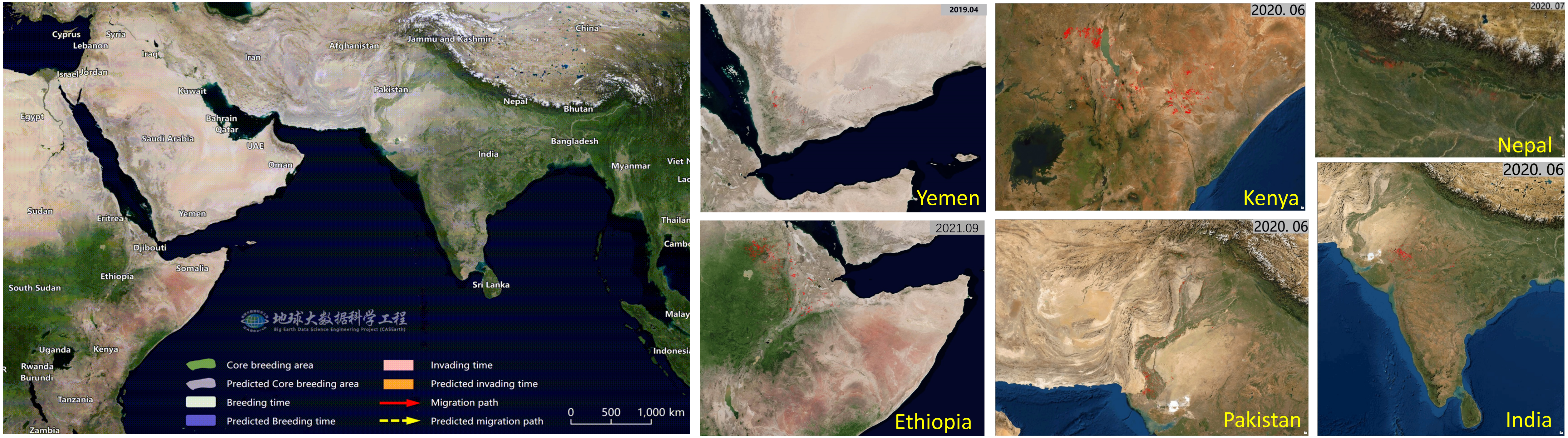

Results of Desert Locust Migration Paths and Disaster Remote Sensing Monitoring in the Asia-Africa Region from 2018 to 2023

Products and Applications

- Using MODIS, Sentinel, SDGSAT-1, and GF satellite data, we have conducted crop disease and pest monitoring and forecasting in major grain-producing countries worldwide. Multiple disaster **monitoring and assessment products** have been released as of now.
- All reports and data have been adopted and globally published by the **Food and Agriculture Organization (FAO)** of the United Nations and the **Global Biodiversity Information Facility (GBIF),** providing decision support for global joint prevention and control of crop diseases and pests. We have received thank-you letters from multiple countries, including **Pakistan, Somalia, and Iraq**. Our achievements have been adopted by the **National Forestry and Grassland Administration**, **the Ministry of Agriculture and Rural Affairs**, and other relevant authorities.

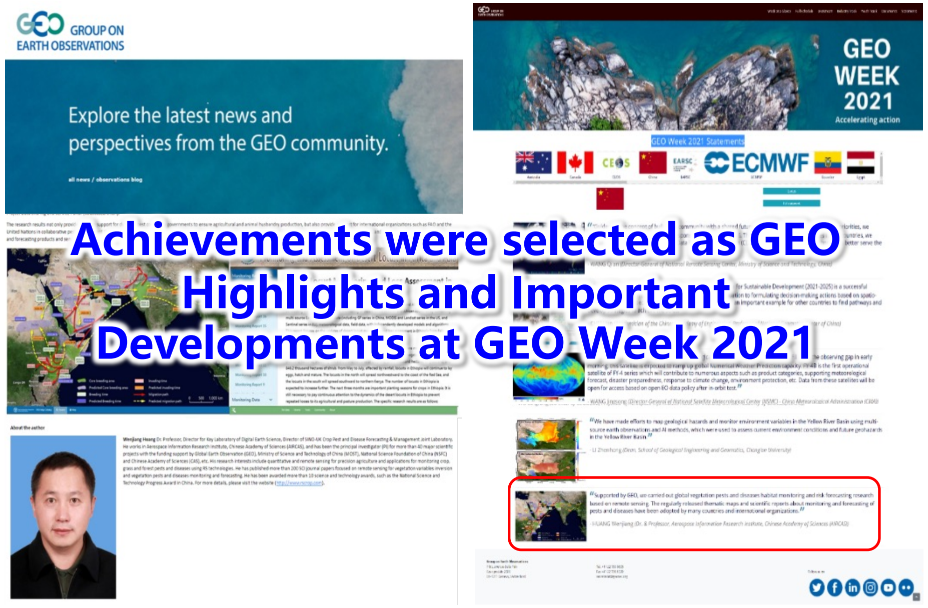

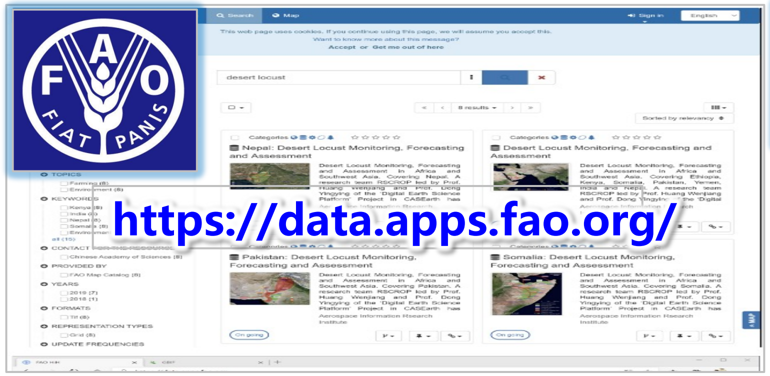

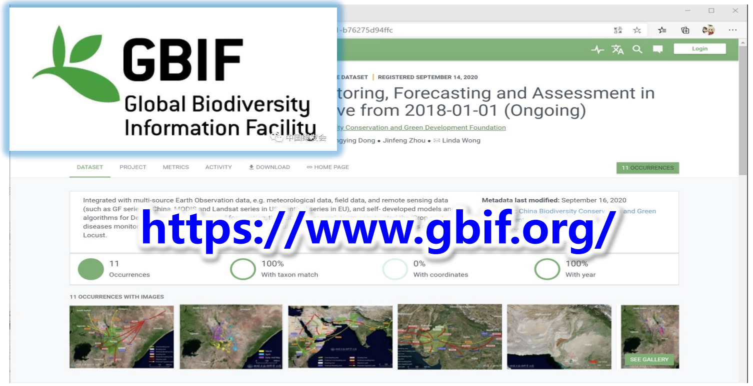

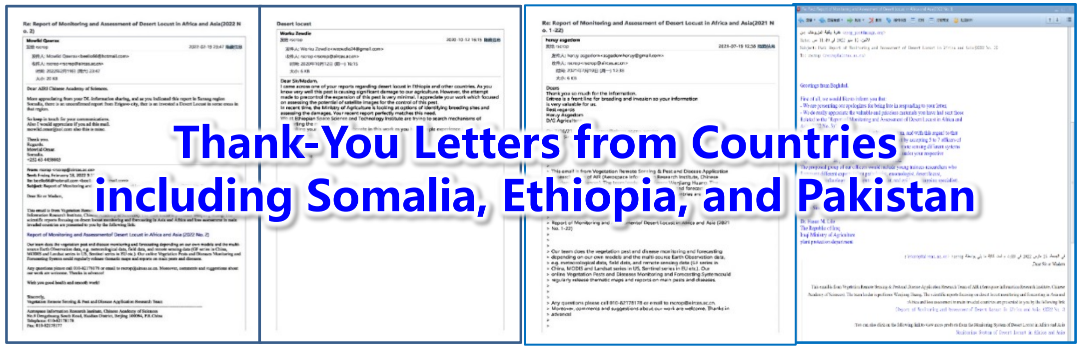

Example(s) of developed service product(s): crop early warning HR

Indicator name	Explanation
CCI	CCI time series based on last 6 years of Sentinel-2 images (actually in production phase)
TAI	Temperature anomalies time series computed from the time of the crop growth starting season
Rain	Precipitation shortage cumulative value starting from one month in advance with respect the crop growth starting season

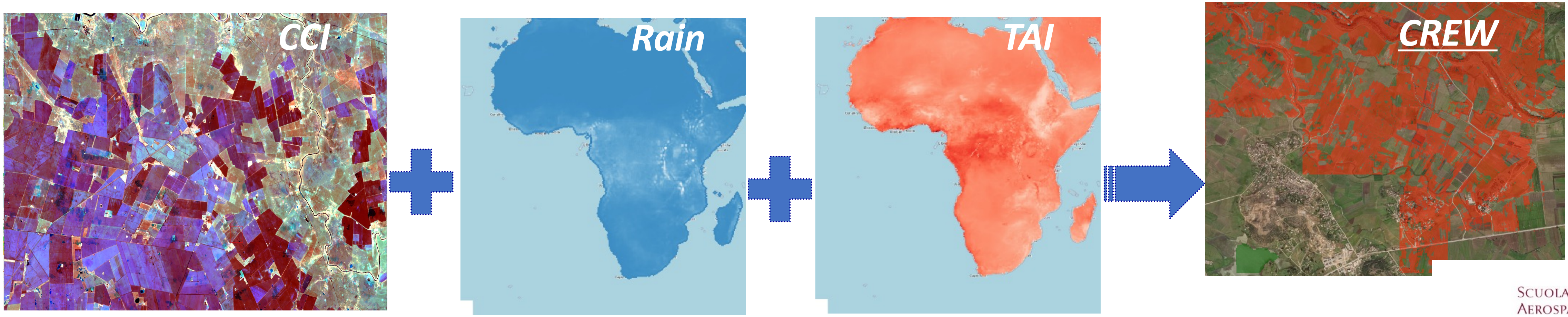

Crop early warning: medium resolution

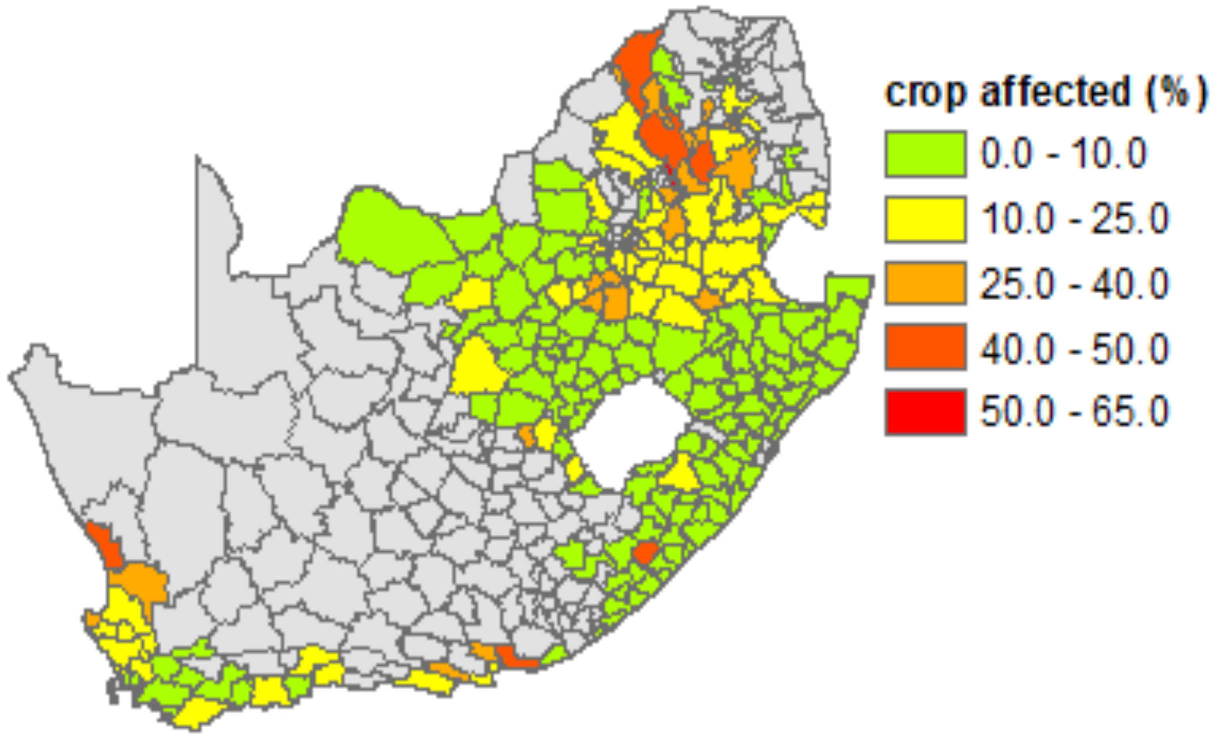

Crop early warning based on NDVI Anomaly, Temperature Anomaly and Precipitation Anomaly, date: 17 May 2021. The figure refers to a low warning due to NDVIA (level of warning = 1). Provinces shown in grey refers to low crop areas (less than 10%).

The service provides maps in geotiff format.

The files contain: an integer number comprised from 1 to 4 corresponding to the level of warning.

The maps are provided on an 8-days frequency with maximum two days delay with respect the last day of the synthesis period.

The output files have the following characteristics:

- Geotiff format.

- Spatial resolution: 250 m. Reference system: WGS 84.

- 1 band.

- Frequency: 8 days

- Band meaning: level of warning. 4 levels of warning are considered: 1 = low warning, occurs when only NDVI anomaly is detected in the period, 2 = medium warning, occurs when NDVI anomaly, accompanied by temperature anomaly, is detected in the period, 3 = high warning occurs when NDVI anomaly, accompanied by precipitation anomaly, is detected in the period, 4 = very-high warning occurs when temperature, precipitation and NDVI anomalies are detected in the period.

- Band 1 range values: 0 – 4, bad value = -1, C

Scuola di Ingegneria Aerospaziale

Sapienza Università di Roma

Relevant Pubblication

F. Rossi et al. Predicting Soil Nutrients with PRISMA Hyperspectral data at the Field Scale: the Handan (south of Hebei Province) test cases. Geo-spatial Information Science Journal, submitted ID 235902087

Mzid, N., Pignatti, S., Huang, W., & Casa, R. (2021). An analysis of bare soil occurrence in arable croplands for remote sensing topsoil applications. *Remote Sensing*, *13*(3), 474.

G. Laneve, S. Saquella, W. Huang and R. Orsi, "Sino-Eu Earth Observation Data to Support the Monitoring and Management of Agricultural Resources," IGARSS 2022 - IEEE International Geoscience and Remote Sensing Symposium, 2022, pp. 4372-4375, doi: 10.1109/IGARSS46834.2022.9884557.

Relevant Pubblication

S. Saquella, G. Laneve and A. Ferrari, "A Cross-Correlation Phenology-Based Crop Fields Classification Using Sentinel-2 Time-Series," IGARSS 2022 - IEEE International Geoscience and Remote Sensing Symposium, 2022, pp. 5660-5663, doi: 10.1109/IGARSS46834.2022.9884724.

M. Kganyago, C. Adjorlolo, M. Sibanda, P. Mhangara, G. Laneve & T. Alexandridis, "Testing Sentinel-2 spectral configurations for estimating relevant crop biophysical and biochemical parameters for precision agriculture using tree-based and kernel-based algorithms", Geocarto International, 2022, DOI: 10.1080/10106049.2022.2146764.

S. Saquella, G. Laneve and A. Ferrari, "A Cross-Correlation Phenology-Based Crop Fields Classification Using Sentinel-2 Time-Series," IGARSS 2022 - IEEE International Geoscience and Remote Sensing Symposium, 2022, pp. 5660-5663, doi: 10.1109/IGARSS46834.2022.9884724.

S. Saquella, A. Ferrari, V. Pampanoni, G. Laneve, Detection Of Irrigated And Rainfed Crops With Machine Learning Multivariate Time-series Object-based Classification Using Sentinel-2 Imagery, IGARSS 2023 - IEEE International Geoscience and Remote Sensing Symposium, 2023.

M. Kganyago, G. Ovakoglou, P. Mhangara, C. Adjorlolo, T. Alexandridis, G. Laneve & J. Suarez Beltran, Evaluating the contribution of Sentinel-2 view and illumination geometry to the accuracy of retrieving essential crop parameters, GIScience & Remote Sensing, 60:1, 2163046, 2023, DOI: 10.1080/15481603.2022.2163046

Zhenhai Li *, Yu Zhao, James Taylor, Rachel Gaulton, Xiuliang Jin, Xiaoyu Song, Zhenhong Li, Yang Meng, Pengfei Chen, Haikuan Feng, Chao Wang, Wei Guo, Xingang Xu, Liping Chen *, Guijun Yang *. Comparison and transferability of thermal, temporal and phenological-based in-season predictions of above-ground biomass in wheat crops from proximal crop reflectance data. Remote Sensing of Environment. 2022, 273:112967.

Yu Zhao, Yang Meng, Shaoyu Han, Haikuan Feng, Guijun Yang*, Zhenhai Li*. Should phenological information be applied to predict agronomic traits across growth stages of winter wheat? The Crop Journal 10 (2022) 1346–1352.

Sun R, Huang W, Dong Y, Zhao L, Zhang B, Ma H, Geng Y, Ruan C, Xing N, Chen X, et al. Dynamic Forecast of Desert Locust Presence Using Machine Learning with a Multivariate Time Lag Sliding Window Technique. Remote Sensing. 2022; 14(3):747. https://doi.org/10.3390/rs14030747

Guo, J.; Lu, L.; Dong, Y.; Huang, W.; Zhang, B.; Du, B.; Ding, C.; Ye, H.; Wang, K.; Huang, Y.; et al. Spatiotemporal Distribution and Main Influencing Factors of Grasshopper Potential Habitats in Two Steppe Types of Inner Mongolia, China. Remote Sens. 2023, 15, 866. https://doi.org/10.3390/rs15030866

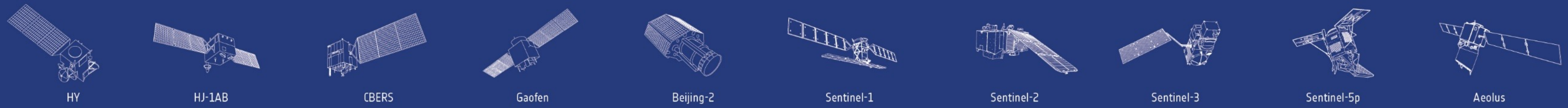
HY
HJ-1AB
CBERS
Gaofen
Beijing-2
Sentinel-1
Sentinel-2
Sentinel-3
Sentinel-5p
Aeolus

THANK YOU